การใช้แบบจำลองทางคณิตศาสตร์เพื่อศึกษาผลของตัวแปรในการทำงานและการแพร่ในแนวรัศมี
ต่อปฏิกิริยาออกซิเดทีฟดีไฮโดรจิเนชันของนอร์มัลบิวเทนในเครื่องปฏิกรณ์แบบเบดนิ่งและเครื่อง
ปฏิกรณ์แบบอิเนิร์ตเมมเบรน

นาย ถาวร เหรียญชลานุสาร

วิทยานิพนธ์นี้เป็นส่วนหนึ่งของการศึกษาตามหลักสูตรปริญญาวิศวกรรมศาสตรมหาบัณฑิต

สาขาวิชาวิศวกรรมเคมี ภาควิชาวิศวกรรมเคมี

คณะวิศวกรรมศาสตร์ จุฬาลงกรณ์มหาวิทยาลัย

ปีการศึกษา 2543

MATHEMATICAL MODELING FOR INVESTIGATING THE EFFECT OF
OPERATING PARAMETERS AND RADIAL DIFFUSION ON OXIDATIVE
DEHYDROGENATION OF NORMAL BUTANE IN THE FIXED BED REACTOR
AND THE INERT MEMBRANE REACTOR

Mr. Tavorn Rienchalanusarn

A Thesis Submitted in Partial Fulfillment of the Requirements
for the Degree of Master of Engineering in Chemical Engineering
Department of Chemical Engineering
Faculty of Engineering
Chulalongkorn University
Academic Year 2000

Thesis Title   Mathematical Modeling for Investigating the Effect of Operating Parameters and Radial Diffusion on Oxidative Dehydrogenation of Normal Butane in the Fixed Bed Reactor and the Inert Membrane Reactor

By   Mr. Tavorn Rienchalanusarn

Department   Chemical Engineering

Thesis advisor   Assistant Professor Suttichai Assabumrungrat, Ph.D.

Thesis co-advisor   Professor Piyasan Praserthdam, Dr.Ing.

_____

Accepted by the Faculty of Engineering, Chulalongkorn University in Partial Fulfillment of the Requirments for the Master's Degree

....Dean of Faculty of Engineering

(Professor Somsak Panyakeow, D.Eng.)

Thesis Committee

....Chairman

(Associate Professor Ura Pancharoen, D.Eng.Sc.)

....Thesis Advisor

(Assistant Professor Suttichai Assabumrungrat, Ph.D.)

....Thesis Co-advisor

(Professor Piyasant Praserthdam, Dr.Ing.)

....Member

(Prasert Pavasant, Ph.D.)

ถาวร เหรียญชลานุสาร : การใช้แบบจำลองทางคณิตศาสตร์เพื่อศึกษาผลของตัวแปรในการทำงาน และการแพร่ในแนวรัศมีต่อปฏิกิริยาออกซิเดทีฟดีไฮโดรจีเนชันของนอร์มัลบิวเทนในเครื่องปฏิกรณ์ แบบเบดนิ่งและเครื่องปฏิกรณ์แบบอิเนิร์ทเมมเบรน (MATHEMATICAL MODELING FOR INVESTIGATING THE EFFECT OF OPERATING PARAMETERS AND RADIAL DIFFUSION ON OXIDATIVE DEHYDROGENATION OF NORMAL BUTANE IN THE FIXED BED REACTOR AND THE INERT MEMBRANE REACTOR) อ. ที่ปรึกษา : ผ.ศ. ดร. สุทธิชัย อัสสะบำรุงรัตน์, อ. ที่ปรึกษาร่วม : ศ. ดร. ปิยะสาร ประเสริฐธรรม ; 92 หน้า. ISBN 974-346-513-8

การศึกษาปฏิกิริยาออกซิเดทีฟดีไฮโดรจีเนชันของนอร์มัลบิวเทนในเครื่องปฏิกรณ์แบบเมมเบรนที่ทำ ด้วยเซรามิก แบบจำลองทางคณิตศาสตร์ได้ถูกนำมาศึกษาถึงประสิทธิภาพของเครื่องปฏิกรณ์ที่สภาวะการปฏิบัติ งานต่าง ๆ ค่าจลนพลศาสตร์ของตัวเร่งปฏิกิริยาวานาเดียมบนแมกนีเซียมออกไซด์ที่ 24wt% V_2O_5 และค่าการแพร่ ของก๊าซผ่านเมมเบรนแบบรูพรุน อัลฟา-อลูมินา (Membralox) ที่มีขนาดของรูพรุน 4 นาโนเมตรได้ถูกใช้ในแบบ จำลอง แบบจำลองทางคณิตศาสตร์ได้พิจารณาถึงสภาวะที่อุณหภูมิไม่คงตัวรวมทั้งผลของการแพร่ในแนวรัศมี ของความร้อนและมวลสาร เนื่องจากปฏิกิริยาออกซิเดทีฟดีไฮโดรจีเนชันของนอร์มัลบิวเทนเป็นปฏิกิริยาคาย ความร้อนค่อนอย่างรุนแรง ปัญหาจุดรวมความร้อนจะเป็นปัญหาหลักที่พบในเครื่องปฏิกรณ์แบบเบดนิ่ง จากการ ศึกษาพบว่าค่าการเลือกเกิดของผลิตภัณฑ์รวมจะเพิ่มขึ้นตามการเพิ่มขึ้นของอุณหภูมิที่ใช้ในการทำปฏิกิริยา นอก จากนั้นปัญหาการเกิดจุดรวมความร้อนและการแพร่ในแนวรัศมีจะพบที่บริเวณทางเข้าของเครื่องปฏิกรณ์ การใช้ เมมเบรนที่ทำด้วยเซรามิกช่วยควบคุมการกระจายของออกซิเจนเข้าสู่บริเวณที่เกิดปฏิกิริยานั้นจะลดปัญหาของจุด รวมความร้อนลงได้มาก จากผลของแบบจำลองยังแสดงให้เห็นถึงอัตราส่วนของอากาศต่อนอร์มัลบิวเทนที่เหมาะ สมสำหรับเครื่องปฏิกรณ์แบบเบดนิ่งและเครื่องปฏิกรณ์แบบเมมเบรน สำหรับเครื่องปฏิกรณ์แบบเมมเบรนอัตรา ส่วนของสารป้อนจะไม่มีผลต่อปัญหาการเกิดจุดรวมความร้อน และเครื่องปฏิกรณ์แบบเมมเบรนจะให้ค่าความ สามารถในการผลิตของผลิตภัณฑ์เหนือกว่าเครื่องปฏิกรณ์แบบเบดนิ่งที่อัตราส่วนของอากาศต่อนอร์มัลบิวเทนมี ค่าสูง ๆ นอกจากนั้นยังแสดงให้เห็นถึงขนาดของเครื่องปฏิกรณ์แบบเมมเบรนที่เหมาะสม จากขนาดของเครื่อง ปฏิกรณ์ที่เหมาะสมนี้เมื่อขนาดของเครื่องปฏิกรณ์เพิ่มขึ้นจะทำให้ค่าการเปลี่ยนของนอร์มัลบิวเทนและค่าการ เลือกเกิดของผลิตภัณฑ์ลดลงทั้งนี้เนื่องมาจากผลของการแพร่ในแนวรัศมี และเมื่อขนาดของเครื่องปฏิกรณ์มี ขนาดเล็กลงการเกิดปฏิกิริยาก็จะลดลงทั้งนี้เป็นผลมาจากการลดลงของปริมาณสารตัวเร่งปฏิกิริยา การเพิ่ม อุณหภูมิที่ผนังของเครื่องปฏิกรณ์ทำให้ค่าการผลิตเพิ่มขึ้นแต่ผลของการแพร่ในแนวรัศมีก็เพิ่มขึ้นเช่นกัน สุดท้าย อุณหภูมิของสายป้อนอากาศจะสามารถควบคุมอุณหภูมิภายในเครื่องปฏิกรณ์ได้

ภาควิชา	วิศวกรรมเคมี	ลายมือชื่อนิสิต	
สาขาวิชา	วิศวกรรมเคมี	ลายมือชื่ออาจารย์ที่ปรึกษา	
ปีการศึกษา	2543	ลายมือชื่ออาจารย์ที่ปรึกษาร่วม	

The oxidative dehydrogenation of *n*-butane in a ceramic membrane reactor was studied. Mathematical models were developed to investigate reactor performance at various operating conditions. Kinetic data of V/MgO catalyst with 24wt% V_2O_5 and permeation data of gases through a porous γ-alumina membrane (Membralox) with 4 nm pore size were used in the models. The non-isothermal condition and radial dispersion of both mass and heat transfer were included in the models. Because the oxidative dehydrogenation of *n*-butane is a highly exothermic reaction, hot spot is a major problem found in conventional fixed-bed reactors. From this study it was found that the selectivity to C_4 hydrocarbon increased with the increase of operating temperature and the hot spot problem and the effect of radial dispersion were pronounced particularly near the entrance of the reactor. The use of the ceramic membrane to control the distribution of oxygen feed to the reaction side could significantly reduce the hot spot temperature. The results also showed that there were optimum feed ratios of air/*n*-butane for the fixed-bed reactor and membrane reactor, however, the hot spot temperature was not sensitive to the feed ratio for the membrane reactor. The membrane reactor outperformed the fixed-bed reactor in term of yield C_4 at high values of the ratio. In addition there is an optimum membrane reactor size. At the optimum reactor size, when the reactor size increased, the conversion of *n*-butane and selectivity to C_4 decreased due to the effect of radial dispersion and when the reactor size decreased, the extent of reaction decreased due to the smaller amount of catalyst. As a result, the yield to C_4 hydrocarbon decreased. It was found that the increase of wall temperature increased the yield but the radial dispersion effect was more pronounced. Finally the feed air temperature was found to be able to control the temperature profile along the reactor length.

Department   Chemical Engineering   Student's signature ....

Field of study Chemical Engineering   Advisor's signature ....

Academic year   2543   Co-advisor's signature ....

ACKNOWLEDGEMENTS

CONTENTS

LIST OF TABLES

LIST OF FIGURES

FIGURE   **PAGE**

Nomenclature

A_C	cross section area	[m^2]
A_{ij}	parameter in equation A-28	[-]
A_{P1}	surface area of reactor at r_1	[m^2]
A_{P2}	surface area of reactor at r_2	[m^2]
A_{P3}	surface area of reactor at r_3	[m^2]
a	Knudsen parameter	$\left[\dfrac{mol \times K^{1/2}}{m \times s \times kPa}\right]$
b	Viscous parameter	$\left[\dfrac{mol \times K}{m \times kPa}\right]$
B	parameter in equation A-31	[-]
C_i	concentration	[mol/m^3]
C_{pi}	heat capacity	[J/(mol K)]
D	equivalent diameter	[m]
$d_{p,m}$	pore diameter of membrane	[m]
D_{er}	effective radial diffusion	[m^2/s]
D_{ij}	diffusion coefficient of binary gas	[m^2/s]
$D_{i,m}$	diffusion coefficient of gas mixture	[m^2/s]
d_p	particle diameter	[m]
E_{ai}	activity coefficient	[J/mol]
E_i	parameter in equation A-9	$\left[\left(\dfrac{g}{mol}\right)^{1/4} P^{-0.5}\right]$
f	friction factor	[-]
F_{Ri}	polar correction	[-]
F_i	molar flow rate	[mol/s]
$\overline{F_i}$	dimensionless molar flow rate	[-]
$F_{T,0}$	total molar flow rate at inlet	[mol/s]
F_c	parameter in equation A-4	[-]
$\left(\dfrac{F_i}{L}\right)'$	molar flow rate of permeate gas I per unit length	[mol/(s m)]

h_{bed}	film heat transfer in catalyst bed	[W/(m^2 K)]
h_{ex}	film heat transfer in tube	[W/(m^2 K)]
H_i	enthalpy	[J/mol]
H_{ij}	parameter in equation A-12	[1/P]
ΔH_{ri}	heat of reaction of reaction i	[J/mol]
J	molar flux	[mol/(m^2 s)]
k_i	rate constant	[mol/(kg s)]
K_i	parameter in equation A-7	[poise]
k_M	thermal conductivity of membrane	[W/(m K)]
k_{SS}	thermal conductivity of stainless steel	[W/(m K)]
L	reactor length	[m]
M	molecular weight	[g/mol]
$\dot{m}$	mass flow rate	[Kg/s]
Nu_{bed}	Nusselt number in catalyst bed	[-]
Nu_{ex}	Nusselt number in tube	[-]
P	Pressure	[kPa]
Pe$_r$	radial peclet number	[-]
Pr	Prandtl number	[-]
r	radial distance	[m]
R	dimensionless of reactor radial length	[-]
Re	Reynolds number	[-]
Re$_{dp}$	packed bed Reynolds number	[-]
r_i	rate of reaction of specie i	[mol/(kg s)]
r_1, r_2	reactor radius	[m]
r_3, r_4	reactor radius	[m]
R_i	rate of reaction of reaction i	[mol/(kg s)]
R_{gas}	Gas constant	[J/(mol K)]
Sc	Schmidt number	[-]
t	time	[s]
T	Temperature	[K]
$\overline{T}$	dimensionless temperature	[-]

$\overline{T_j}$	dimensionless reactor wall temperature	[-]
T_v^*	parameter in equation A-3	[-]
T_D^*	parameter in equation A-17	[-]
T_{rij}	parameter in equation A-13	[-]
u	gas velocity	[m/s]
U_i	parameter in equation A-8	[-]
U_M	overall heat transfer coefficient through membrane	[W/(m^2 K)]
U_{SS}	overall heat transfer coefficient through stainless steel	[W/(m^2 K)]
W/F	mass of catalyst per molar flow rate of gases	[kg s/mol]
y_i	mole fraction	[-]
z	length	[m]
$\overline{Z}$	dimensionless length	[-]

Greek Symbols

ρ	density of gas	[kg/m^3]
ρ_B	density of catalyst	[kg/m^3]
τ_g	tortuosity	[-]
ε	porosity	[-]
ε_r	emissivity of solid	[J/(m^2 s K^4)]
κ	special correction for high polar substance	[-]
μ	viscosity	[P]
φ_{tr}	monatomic value of the thermal conductivity	$[\frac{K^{1/6}g^{1/2}}{Pa^{2/3}mol^{1/2}}]$
α	dimensionless mole balance parameter	[-]
α_{rs}	radiation coefficient for the solid	[J/(m^2 s K)]
β	dimensionless energy balance parameter	[-]
λ	thermal conductivity	[W/(m K)]
λ_{er}	effective radial thermal conductivity	[W/(m K)]
λ_{er}^0	static effective radial thermal conductivity	[W/(m K)]

λ_{er}^t	dynamic effective radial thermal conductivity	[W/(m K)]
γ_1	the ratio of inlet temperature tube side to shell side	[-]
γ_2	the ratio of inlet temperature shell side to tube side	[-]
η	dipole moment	[debye]
η_r	dimensionless dipole moment	[-]
η_{rij}	equation in equation A-14	[-]
ω	acentric factor	[-]
θ_0	selective oxidation site	[-]
λ_0	non-selective oxidation site	[-]
v_i	stoichiometric coefficient	[-]
Λ	parameter in equation A-30	$[\dfrac{K^{1/6}g^{1/2}}{Pa^{2/3}mol^{1/2}}]$
Γ	wetted perimeter	[m]
Ω_v	viscosity collision	[-]
Ω_D	diffusion collision	[-]
σ	Lennard-Jones parameter	[A]
σ_{ij}	characteristic length	[A]
δ	parameter in equation A-18	[-]
$\dfrac{\varepsilon}{k}$	parameter in equation A-19	[K]
δ_{ij}	parameter in equation A-21	[-]
$\dfrac{\varepsilon_{ij}}{k}$	parameter in equation A-22	[K]
θ	parameter in equation A-30	[-]

Subscript

0	inlet condition
1	feed side
2	permeate side

b   normal boiling point

c   critical condition

f   feed

FBR   fixed bed reactor

g   gas

IMR   inert membrane reactor

k   Knudsen flow

m   mixture gas

r   reduce

s   shell side

sc   solid catalyst

t   tube side

T   total

v   Viscous flow

w   wall of reactor

Superscript

s   shell side

t   tube side

CHAPTER I
INTRODUCTION

Light olefins are very useful commodities in petrochemical industry. The conversion of paraffins to olefins is an important way to increase the chemical value of paraffins. The synthesis of light olefins for the petrochemical industry is mainly carried out through the processes of steam cracking and fluid catalytic cracking (FCC) of natural gas and oil fractions, as well as by paraffin dehydrogenation. The dehydrogenation makes it possible to obtain specific olefins for use in the polymer and intermediates industries. However, the dehydrogenation suffers from some drawbacks, being an endothermic reaction, favourable at high temperature and thermodynamically limited by equilibrium. High energy cost is associated with the furnishing of heat at the high temperatures of reaction. In addition, coke formation favours under such condition and, consequently, the catalysts need frequent regeneration.

An alternative process employs oxidative dehydrogenation reaction which is exothermic, unlimited by equilibrium and resistant to coke formation. However, the oxidative dehydrogenation has some problems which are responsible for the lack of commercial application. These are

1. The valuable co-product hydrogen is lost by being transformed to water.
2. Low selectivity is generally achieved as the nature of hydrocarbons that alkane is more inert than alkene. Thus, at high partial pressure of oxygen any catalyst that can oxidize alkane can also activate alkene to react further with oxygen into combustion products of carbon oxides and water. Among several systems investigated, vanadium supported on magnesium oxide (V-Mg-O) has received more attention than any others in the oxidative dehydrogenation because of its high selectivity to alkene.

3. Finally, the hot spot is formed near the entrance of a fixed-bed reactor because of the high exothermicity and high concentration of oxygen.

To solve these problems, apart from the development of better-performance catalyst, a number of non-traditional reactors have been developed such as a fixed-bed reactor with multiple feed inlet of oxygen, a monolith reactor, a catalytic membrane reactor, etc. In recent years an inert membrane reactor (IMR) is one of the non-traditional reactors of interest. The application of membrane reactors is to introduce a reactant in a controlled manner in a reacting network where several reactions are possible. The researches on this application have been increasing in these few years because the membrane permselectivity is a less urgent needed.

Many oxidative dehydrogenation reactions have been studied in the inert membrane reactor such as ethane (Coronas *et al.,* 1995a), propane (Ramos *et al.,* 2000) and *n*-butane (Tellez *et al.,* 1997). The use of the ceramic membrane to distribute the oxygen feed to the reaction zone could help improve the selectivity obtained at a given hydrocarbon conversion by lowering the oxygen partial pressure in the reaction zone. This can also avoid the flammability mixture due to segregated feed and control average oxidation state of catalyst in the reactor. In addition, the heat is distributed more evenly along the bed, thereby decreasing the formation of hot spots and the probability of runaway behavior.

Although a number of researchers studying the oxidative dehydrogenation in the inert membrane reactor but most of them did not take into account the radial diffusion effect except Tonkovich *et al.* (1996a) who found that the reactions occurred predominately near the membrane wall. From the above reasons, this research focused on the development of mathematical model for the oxidative dehydrogenation. The non-isothermal condition and radial dispersion effect were included in the model. The oxidative dehydrogenation of *n*-butane was used as an example reaction. The objectives of the study are to investigate

1. The performance of oxidative dehydrogenation of *n*-butane in the inert membrane reactor compared with the fixed-bed reactor.
2. The effect of radial dispersion on the reactor performance.
3. The effect of operation parameters such as air/*n*-butane ratio, size of reactor, wall temperature reactor and feed air temperature.

CHAPTER II
LITERATURE REVIEWS

The incorporation of membranes into reactors is an interesting process. There are a number of review papers (e.g. Armor, 1998; Gryaznov, 1999; Santamaria *et al.,* 1999; Saracco *et al.,* 1999; and Soria, 1995) addressing the development in this field. In general, the recent publications on membrane reactors focused on overcoming the problem of the reaction, which is equilibriumly limited by selective removal of one or more products through the membrane. The other field of application is based on selectivity enhancement which can be carried out by selective removal of an intermediate product or controlled dosing a reactant through the membrane. In this chapter some of the developments and outstanding opportunities in the field of catalytic reactors based on inorganic membrane will be provided.

2.1 Types of membranes

Membranes can be classified broadly based on the materials into organic and inorganic membranes. The first widespread use of polymer membranes for separation applications dated back to the 1960-70s when cellulose acetate was casted for desalination of sea and brackish waters. However, cellulose acetate membranes had limited pH, temperature and chlorine tolerance range. This led to the development of the second generation of organic membrane made of polymer materials. Since then many new polymer membranes came to the commercial applications on ultrafiltration (UF), microfiltration (MF), reverse osmosis (RO), dialysis, electrodialysis and gas separations. The choice of membrane materials is dictated by type of application, environments, separation mechanisms for which they operate and economic considerations. Table 2.1 lists some of the common organic polymer materials for various membrane processes. They include, in addition to cellulose acetate, polyamides, polyimides, polysulfones, nylons, polyvinyl chloride, polycarbonate and fluorocarbon polymers. However, the disadvantages of organic membranes are their

low thermal stability, poor mechanical strength, problems of compacting and swelling, poor resistance toward chemicals and cleaning problems. As a result, development of membrane made of inorganic materials such as metals, ceramics, and inorganic polymers has been carried out.

Table 2.1 Commonly used organic membrane materials and their properties.

Materials	Applications	Approximate maximum Working temperature (K)	pH range
Cellulose acetates	RO, UF, MF	323	3-7
Aromatic polyamides	RO, UF	333-353	3-11
Fluorocarbon polymers	RO, UF, MF	403-423	1-14
Polyimides	RO, UF	313	2-8
Polysulfone	UF, MF	353-373	1-13
Nylons	UF, MF	423-453	
Polycarbonate	UF, MF	333-343	
Polyvinyl chloride		393-413	
PVDF	UF	403-423	1-13
Polyphosphazene		448-473	

Inorganic membranes were industrially developed five decades ago with the aim of separation of UF$_6$ using gas phase diffusion processes. In the 1980s, non-nuclear industrial applications were in place mainly oriented towards microfiltration and ultrafiltration processes. The application of porous ceramic membranes as catalytic reactors also was started in the 1980s. The driving force for this change was the possibility of integrating reaction and separation in a single unit operation. This concept had already been achieved in the field of biochemical engineering using polymer membranes. These membranes, however, were not suitable for applications in chemical processes which employ high temperature or harsh conditions. The

intense research activities on the development of inorganic membranes have made possible the implementation of the membrane reactor concept to the high operating temperature area.

Inorganic membrane can be categorized into two groups, namely dense (nonporous) and porous inorganic membranes. Dense membranes are mainly made of thin metal or oxide films such as palladium and its alloys, zirconia and pervskite material. The nonporous metallic membranes are known to provide high selectivity since they are selectively permeable to certain gases. For example, palladium based membranes are permeable only to hydrogen (Lee *et al.,* 1994) while zirconia and pervskite material are well-known to be permeable only to oxygen (Xu *et al.,* 1999 and Thomson *et al.,* 1999). For the use of membrane reactors to control the reactant feed, such as oxidative dehydrogenation reaction, although dense membranes are selectively permeable, the modest oxygen fluxes involve, resulting in low hydrocarbon conversion and therefore low yield per pass. In addition, the dense membranes is limited by their brittleness tendency, high cost and low permeability compared to microporous membrane.

Porous membranes are superior to dense membranes from the point of view of their permeability; nevertheless, the selectivity of the porous membranes is not as good as that of the dense membranes. Today commercialized inorganic membranes are dominated by porous membranes and particularly by porous ceramic membranes. Porous ceramic membranes can be made, in whole or in part, of alumina, silica, titania, zirconia, zeolites, etc. Commercial ceramic membranes currently in use usually have an asymmetric structure consisting of a support layer (generally α-alumina) with large pores and a low pressure drop, and a separation layer made of a different material (γ-alumina, zirconia, silica, etc.), which controls the membrane permselectivity.

Because this type of membrane is commercially available now. A number of research has extensively employed the porous ceramic membranes in various catalytic reactions such as dehydrogenation (e.g. Koukou *et al.,* 1996; Gobina *et al.,* 1995a;

Schramm *et al.,* 1999), oxidative dehydrogenation (e.g. Ramos *et al.,* 2000) and oxidative coupling of methane (e.g. Miguel *et al.,* 1996).

A composite membrane is a new generation of membrane. It compromises advantages of dense and porous membranes to obtain moderately high fluxes and high selectivities. The composites consist of a porous support superimposed with a thin selective membrane layer (dense metal or dense oxide). The preparation methods are such as sol-gel (Lee *et al.,* 1994), electroless plating (Cheng *et al.,* 1999) and chemical vapour deposition (CVD) (Xomeritakis and Lin, 1998). Although composite membranes hold the promise of a selectivity equivalent to that of dense membranes at higher permeation fluxes but it is still at fundamental research level.

2.2 Membrane reactors

Major application areas of membrane reactors can be classified into two types. The first is yield enhancement that is the most common application opportunity of membrane reactors for a chemical equilibrium limited reaction. The higher conversions compared to conventional fixed-bed reactors can be achieved by having one or more of the reaction products diffusing out of a semipermeable membrane surrounding the reacting mixture. As a result, the reaction will continue to proceed toward completion. Dehydrogenation reactions including other reactions such as decomposition and production of synthesis gas are main reactions in the application area.

The second application of membrane reactor is selectivity enhancement. The reaction in this application are consecutive and series-parallel reactions (e.g. partial oxidation). Achievement of selectivity enhancement is carried out by selective removal of intermediate product or controlled addition of a reactant. In the first case, an intermediate product, which is mostly the desired product, is removed from the reaction chamber. As a result, subsequent reactions which consume the intermediate product can be suppressed. However, because the molecular size of the product is usually larger than the other gas species, it is difficult to be removed from the system.

Consequently, this type of application is not widely under investigation. (Bernstein *et al.,* 1993).

Another way to increase the selectivity is the controlled addition of a reactant. In the recent year, a number of the researches have been carried out in this field because the membrane permselectivity is a less urgent need (if any) for this kind of applications. The controlled addition of an reactant (e.g. oxygen, hydrogen) through membrane to the reaction zone can keep the partial pressure in the reaction zone at low value. This increases the selectivity to a desired product. Examples of reactions in this case are partial oxidation, oxidative coupling and oxidative dehydrogenation.

2.2.1   Membrane reactor for yield enhancement

Most of the application in this field has often focused around the selective separation of H_2 from the reaction chamber by using either a metal membrane or a microporous membrane with high selectivity to hydrogen separation. The following reviews are present to each of the reaction that produces H_2 as a co-product.

The steam reforming of methane is the most important process for the industrial manufacture of hydrogen from light hydrocarbons. It is a very endothermic reaction that operates at about 1027 K and 2.026×10^3 kPa in order to achieve near equilibrium conversions and to meet the customers need for high pressure H_2. By incorporating a Pd alloy membrane into the reaction system the reaction can proceed to produce more H_2 at lower operating temperatures. In addition, the use of the Pd based membrane could produce H_2 with higher concentration, thus simplifying the current operation. Uemiya *et al.,* (1991) studied steam reforming of methane by using an alumina supported Ni catalyst contained within an 80 μm Pd on Pd/23% Ag alloy membrane coated onto a porous glass tube. At the steam/CH_4 ratio of 3, they achieved the conversion of CH_4 approaching 80% at 101.3 kPa and 773 K compared to the equilibrium value of about 42%. Barbieri *et al.,* (1997) also considered this reaction using a mathematical model of dense Pd membrane reactor. The effects of various operating parameters were studied and they found that the countercurrent-flow

configuration at high temperature is advantage over the co-current flow configuration. At low temperature, the countercurrent flow configuration gives a lower performance than the co-current flow one because of the inversion of hydrogen permeation flux. Kikuchi (2000) employed non-palladium membranes (such as Pt) prepared by CVD method. Higher conversion of methane than thermodynamic equilibrium was obtained.

Another way to produce syngas is partial oxidation of methane. Galuszka *et al.,* (1998) showed that the use of dense palladium membrane can increase the methane conversion between 4-20 % and CO and H_2 yield between 2-20 % and 8-18 %, respectively. However, they also found that filamentous carbon can be formed on the palladium membrane and membrane swelling leads to its destruction. Because partial oxidation of methane is a mass-transport limitation, the uses of fluidized bed and fluidized bed membrane reactor to give a higher yield of syngas were studied (e.g. Mleczko *et al.,* 1996; Ostrowski *et al.,* 1998a and1998b).

For the application of membrane reactor on dehydrogenation reactions, since they are endothermic reactions and experience equilibrium limitation, conversion is favored at high temperature which reduces selectivity and leads to catalyst deactivation by coking. By using membrane reactor to remove hydrogen product, the same conversion could be obtained at lower operating temperature thereby reducing undesired reactions.

Classical works of Itoh *et al.,* (1987) and Gryaznov *et al.,* (1986) led the way for others to build small membrane reactors for the dehydrogenation of alkanes. Itoh and coworkers studied dehydrogenation of cyclohexane to benzene by using 1.27 mm thick Pd/Ag membrane tube containing a 0.5% Pt/Al_2O_3 catalyst. The operating condition was 473 K and 101.3 kPa. Argon was used as both a sweep gas and a carrier gas for saturated cyclohexane vapour. They found that the conversion of cyclohexane can achieve 99%. Kikuchi and coworkers (1995) extended this work into a number of other reactions. The membranes were made of a Pd alloy coated onto a mesoporous membrane support. Isobutane was passed over a Pt/Al_2O_3 catalyst, the yield of

isobutylene increased from the equilibrium value of 6% to 23% at 673 K with the presence of membrane. They reported some deactivation of membrane that was due to carbon buildup on the catalyst and the rate of H_2 production was limited by catalyst activity. For the mesoporous alumina and a microporous zeolite membrane reactor systems Casanave *et al.,* (1995) reported higher conversion when compared to a convention reactor. However, these increases were related to two different phenomena: a complete mixing of reactants, products and sweep gas in the case of mesoporous membrane and a continuous separation H_2 when the microporous zeolite membrane was used. Casanave *et al.,* (1999) also used the same reaction with zeolite membrane to study performance under the co-current and the countercurrent modes. They found that although the separation factor was higher in countercurrent than in co-current, the yield of reaction in these two sweeping modes was almost the same.

Collins *et al.,* (1996) studied the dehydrogenation of propane using a Pd film coated on a mesoporous Al_2O_3 support in a device containing a commercial Amoco dehydrogenation catalyst. Propylene yields increased from the equilibrium value of 30% to 40% at 823 K and propylene selectivity was above 97%. They also reported catalyst deactivation due to carbon deposition on the catalyst. Another dehydrogenation reaction of interest in the petrochemical industry is the ethylbenzene dehydrogenation to styrene. Quicker *et al.,* (2000) used palladium composite membranes on an asymmetric ceramic tube to achieve the increased of styrene yield above 15%.

The further intriguing application opportunity is the coupling of reactions at the opposite membrane sides. A typical case study is the contemporary handling of a dehydrogenation on one side of the membrane and a hydrogenation on the other side. This operation mode could enhance the per-pass conversion of both reactions. Moreover, the exothermic reaction could in principle supply the heat required for the endothermic one. Despite these potential benefits, little experimental study has been addressed to this last topic in recent years. Gobina *et al.,* (1996), studied the catalytic dehydrogenation of *n*-butane in membrane reactor made of a 6 μm Pd/Ag film by performing experiment and modeling. Uses of inert (N_2) and reactive sweep gases

(N_2/CO and N_2/O_2) enhanced the conversion to be the value of 5 to 8 times above the equilibrium one. Itoh and Wu (1997) focused on the thermal sustainment obtained from the oxidation of the permeated hydrogen from the endothermic cyclohexane dehydrogenation occurring at the opposite membrane side. Considerable energy savings compared to indirect heating of the reactor were proved. Hermann *et al.,* (1997) compared the results of ethylbenzene dehydrogenation in a composite palladium membrane under various process configurations; i.e. the use of inert sweep gas, evacuation of the permeation gas, and oxidation of the permeated hydrogen. The results showed that the oxidation of the permeated hydrogen with air seems to be more effective than the application of inert sweep gas or vacuum.

Finally, several environmental-related reactions were attempted by using permselective membrane reactors. Ammonia decomposition into nitrogen and hydrogen from coal gasification streams was successfully tested by Collins and Way (1994) over Pd-Ag membranes. The measured conversion at 823 K in a membrane enclosed fixed-bed reactor of a Ni-Al$_2$O$_3$ catalyst was 79% instead of 17%, measured for a standard reactor. Similar results were obtained for other high-temperature decompositions of noxious gases such as H$_2$S by selective permeation of hydrogen through Pt-V membranes (Edlund and Pledger, 1994).

2.2.2   Membrane reactor for selectivity enhancement

Most applications on the improvement of reaction selectivity involve consecutive or series-parallel reaction such as partial hydrogenation and partial oxidation. The lower partial pressure of H$_2$ or O$_2$ in the reaction zone can prevent the formation of total oxidation or hydrogenation product. The following reviews provide the details of works on this application.

Controlled addition of hydrogen

Partial hydrogenation of multiple unsaturated hydrocarbons is an important process in the petrochemical industry. It is used in both the purification of alkene feed streams and the production of commodity chemicals from alkynes and aromatics. Since dense palladium membrane are highly permselective to H_2 gas, they have been employed in many reaction systems. Pd/Ni membrane (Gryaznov *et al.,* 1982), Pd, Pd/Ru and Pd/Ag membranes (Itoh *et al.,* 1993) were used in the partial hydrogenation of acetylene at 373 K. They found that the permeate hydrogen was very active to hydrogenation of acetylene in which ethylene was the desired product.

The organometallic membranes such as Pd-polymer membrane is also attractive in this field. Liu *et al.,* (1998) used the catalyst consisting of polymer-anchored palladium on the inside wall of cellulose acetate or polysulfone fibers, for the selective hydrogenation of butadiene in crude 1-butene at 313 K. The selectivity of nearly 100% to 1-butene under mild reaction condition was obtained. Ciebien *et al.,* (1999) also used the organometallic of Pd to study the same reaction. This study showed that palladium nanoclusters synthesized within diblock copolymer films were active and selective catalysts for the partial hydrogenation of 1,3-butadiene, even though the clusters were completely surrounded by a bulk polymer matrix. The overall selectivity for butenes, and particularly the selectivity for 1-butene, increased with decreasing hydrogen partial pressure as the rate of 1-butene hydrogenation was reduced. In addition, the lower temperature favored formation of 1-butene over 2-butene.

Lambert *et al.,* (1999) studied this reaction in a Pd/γ-Al_2O_3 catalytic membrane of acetylene and 1,3-butadiene. The hydrogenation reaction performed by flowing a premixed feed through the Pd/Al_2O_3 membrane wall provided the highest selectivity to partially hydrogenated product while maintained a high conversion without any loss of hydrocarbon species.

The controlled addition of oxygen

The most famous reactions in these applications were oxidative coupling of methane (OCM) and oxidative dehydrogenation (ODH).

The oxidative coupling of methane is interesting because the abundance of natural gas makes methane, its major component, a raw material of great synthetic importance. To use this natural resource in chemical, petroleum and energy industries, methane should be converted on site to more easily transportable and active chemical or fuel (e.g. ethylene or methanol). One of the more recent and potentially attractive prospects is the oxidative coupling of methane to higher hydrocarbons product (main product is C_2). Lafarga *et al.,* (1994b) used the porous ceramic membrane enclosed with Li/MgO catalyst bed to study this reaction. The results showed that the oxygen distribution can significantly improve the selectivity of C_2. The same membrane was employed by a number of researches such as Miguel *et al.,* (1996) and Tonkovich *et al.,* (1996b). Miguel and co-worker used many types of catalysts in the study (Li/MgO, Li/Sn/MgO, Li/Na/MgO, Na/W/Mn/SiO$_2$, etc.). In most cases, the ceramic membrane reactor provided significant advantages over the conventional fixed-bed reactor, over a wide interval of conversion. However, the extent of the improvement that can be obtained with the inert membrane reactor depends on the kinetics of the particular system employed, which in turn is a function of the nature of the catalyst and the conditions employed. Tonkovich and co-workers (1996b) used samarium oxide doped magnesium oxide catalyst to study using both mathematical model and experiment. The results showed that the membrane reactor outperformed the fixed-bed reactor when the rate constant for the desired reaction exceeded that of the undesired reaction. The samarium oxide catalyst enclosed with vycor membrane was studied by Ramachandra *et al.,* (1996) and the results were similar to the previous.

Another type of membrane for the oxidative coupling of methane was a dense oxide membrane. A mathematical model was developed by Wang and Lin (1995) to study the reaction in a dense oxide membrane. The results showed a possibility of achieving much higher C_2 yields (>70%) for the OCM in the dense oxide membrane

reactors than in a conventional fixed-bed reactor. Xu and Thomson (1997) also studied this reaction in a dense solid oxide membrane using the experimental. They obtained C_{2+} selectivities of 50% at 1098 K which is significantly by higher than those from a fixed-bed reactor. The results also indicated that permeability of this material appeared to be limited by high oxygen ion recombination rate in perovskite membrane. This also indicated that oxygen fluxes are not limited by diffusion, but by surface exchange rate. Zeng *et al.,* (1998) used the perovskite membrane with one membrane surface exposed to O_2/N_2 mixture stream and the other to CH_4/He mixture stream. At temperature higher than 1123 K, high C_2 selectivity (70-90 %) and yield (10-18 %) were achieved with a feed ratio (He/CH_4) of 40-90. The C_2 selectivity dropped dramatically to less than 40% as the He/CH_4 ratio decreased to 20.

Oxidative dehydrogenation is another way to produce unsaturated hydrocarbon (alkene and alkyne) unlike direct removal of H_2 gas from saturated hydrocarbon as dehydrogenation reaction. The advantages of this process are that the reaction is unlimited by thermodynamic equilibrium, energy saving because the reaction is very exothermic and tolerated to catalyst deactivation because O_2 and H_2O appeared in the system. However, this reaction also has some drawbacks on low selectivity and formation of hot spot. One way to improve the oxidative dehydrogenation reaction is development of good performance catalyst. Many researches have been carried out using various catalysts such as V-base catalysts (Blasco et al., 1995; Nieto et al., 1999) and Mo catalysts (Martin-Aranda et al., 1995; Vrieland and Murchison, 1996; Dejoz et al., 1999). Probably the best catalyst obtained to date was V-Mg-O catalyst with high selectivities to olefin (Valenzuela *et al.,* 1995; Nieto et al., 1998; Lemonidou *et al.,* 1998; Tellez *et al.,* 1999b).

In the recent years another approach to improve the performance of the reactions has been focused on the use of non-traditional reactors such as monolith reactors, catalytic membrane reactors and inert membrane reactors. Capannelli *et al.,* (1996b) studied the oxidative dehydrogenation of propane and compared a fixed-bed reactor with a monolith reactor. They found that as the residence time or propane conversion increased, the selectivity to propylene was almost constant unlike the

fixed-bed reactor whose the selectivity decreased rapidly. This effect can be explained that the diffusion of propylene into the pores of the catalyst grains in the fixed-bed reactor was responsible for the consecutive reactions of olefin combustion. In addition, they formed that when oxygen is a limiting reactant, the selectivity to propylene is higher than the case of excess oxygen.

Capannelli *et al.,* (1996a) and Alfonso *et al.,* (1999) compared the performance of three types of reactors i.e. fixed-bed, monolith and catalytic membrane reactors. They found that CMR gave slightly higher selectivity to propylene than the monolith reactor because of the higher HC/O_2 ratio. A number of researchers (Alfonso *et al.,* 1999; Capannelli *et al.,* 1996a and Pantazidis *et al.,* 1995) used the CMR to study this reaction. The results showed that feeding alkane to the catalytic side and O_2 in the opposite side gave higher selectivity than feeding O_2 and propane in the catalyst side. Moreover, feeding an inert gas with alkane in the catalyst side gave lower selectivity because of the increased partial pressure of O_2 in catalytic layer. Alfonso *et al.,* (2000) also used the CMR with two types of catalytic membranes made of V/MgO and V/Al_2O_3 membranes. The results showed that the V/MgO membrane was more selective but less active than the V/Al_2O_3 membrane in the temperature range of 773-833 K. Because catalyst was deposited on membrane for the CMR, the change of the catalyst would require the change of membrane material as well. Alfonso *et al.,* 2000 and Ramos *et al.,* 2000 found that the IMR had a higher yield than the CMR.

The IMR has drawn a number of interest in the recent years. Many reactions have been studied, for example, the oxidative dehydrogenation of ethane (Al-Sherehy *et al.,* 1998; Coronas *et al.,* 1995a; Tonkovich *et al.,* 1995 and Tonkovich *et al.,* 1996a), propane (Pantazidis *et al.,* 1995 and Ramos *et al.,* 2000) and *n*-butane (Tellez *et al.,* 1997 and 1999a). All researchers found that the distribution of O_2 feed by using membranes increased the reactor performance. Tonkovich *et al.,* (1995 and 1996a) performed experiment at 873 K at long residence times and found that the membrane reactor always produced higher ethylene yields than fixed-bed reactors at low C_2H_6/O_2 feed ratios. As the feed ratios increased, the yields of two reactors reached

the same value. At the shorter residence times, an inversion sometimes occured where the fixed-bed reactor outperformed the membrane reactor at the higher feed ratio. The membrane had a significant effect when the feed of reactant was highly O_2 contained (Pantazidis *et al.,* 1995; Tonkovich *et al.,* 1995 and 1996b; Tellez *et al.,* 1997 and 1999a).

Tellez *et al.,* (1997) and Ramos *et al.,* (2000) showed that feeding of inert gas with O_2 in the permeation side had a main disadvantage related to the formation of coke and cracked products in the entrance region of the reactor. From the works of Tellez *et al.,* (1997 and 1999a) by experiment and mathematical modeling, they also showed that the permeation of O_2 to the catalyst bed can improve the oxidation state of catalyst. This was a reason that the membrane reactor outperformed the fixed-bed reactor.

The controlled addition of O_2 does not only improve the selectivity but also avoids the explosion mixture. As a result, wider range of operation condition can be carried out without hot spot formation. Because the reaction was gradually take place evenly in all part of the catalyst bed unlike in the fixed-bed reactor in which most of the reaction was taken place near the feed entrance (Coronas *et al.,* 1995a; Coronas *et al.,* 1995b; Tonkovich *et al.,* 1996a; Tellez *et al.,* 1997 and Al-Sherehy *et al.,* 1998).

The oxidative dehydrogenation of *n*-butane (ODB) in an inert Al_2O_3 membrane was studied by Tellez *et al.,* 1997. They showed that the membrane was not significantly degraded after work. In general, a porous ceramic membrane was used in the membrane reactors for controlled addition of O_2. Some researchers focused on the modification of the porous structure of the membrane (Lafarga *et al.,* 1994a; Ramos *et al.,* 2000; Coronas *et al.,* 1995a; and Tellez *et al.,* 1997). The modification was made by impregnation with a commercial silica or boehmite sol to decrease its permeability to more adequate value for the purposes. In some cases, the membrane was impregnated with base solution such as lithium or sodium nitrate solution to reduce the acidity of membrane, because the acidity of membrane is responsible for cracking reaction of alkane and alkene. In addition, the basicity of

alkene trends to let it adsorb on acidic membrane surface where deep oxidation to carbon oxide takes place. As a result the reduction of acidity of membrane can reduce deep oxidation of alkene.

2.2.3   Mathematical model development

The applications of membrane reactor for selectivity enhancement have been increased in the past few years. Besides the experimental work, some efforts have been focused on the computer simulation. Because of the relatively new concept on the controlled addition of reactants, there have been just a few workers investigating the benefits of a distributed feed in a chemical reactor by using the mathematical modeling. The basic assumptions such as steady state, isothermal, isobaric and plug flow condition are generally applied to simulate an inert membrane reactor (Tonkovich *et al.,* 1996b; Kao *et al.,* 1997) and an catalytic membrane reactor (Wang and Lin 1995; Lu *et al.,* 1997). All of them found that the membrane reactor provided better performance than the fixed-bed reactor. Kao *et al.* (1997) shows that the isothermal fixed-bed reactor model of the oxidative coupling of methane provided a reasonable prediction of the experimental results. The simulation results for the 3% Li/MgO catalyst fitted the experimental results quite well. However, the prediction on the 7% Li/MgO catalyst case was lower than the experimental values. They postulated that the actual reactor may not be operated under the isothermal condition. Some researchers (Coronas *et al*., 1995a; Coronas *et al*., 1995b) found that the temperature in the inert membrane reactor and the fixed-bed reactor for an exothermic reaction was not isothermal and the formation of hot spot was found near the entrance of the reactors. Then the energy balance was generally taken into account in the mathematical modeling. Al-Sherehy *et al.* (1998) developed a non-isothermal mathematical model to evaluate the performance of the catalytic oxidative dehydrogenation of ethane to ethylene. The reactor included a distributor tube with a desired number of holes located in the catalyst bed to distribute the feed oxygen. This model simulated the operation under non-isothermal and plug flow condition. They found that the hot spot temperature was significantly reduced with increasing the number holes but it could not improve the selectivity. Tellez *et al.,* (1999a) also

developed a mathematical model including the energy balance and pressure drop in a catalyst bed to evaluate the performance of the oxidative dehydrogenation of normal butane in an inert membrane reactor. They found that the simulation results agreed with the experimental results. In addition, the membrane reactor could improve the selectivity by improving the catalyst selectivity site and reducing the hot spot temperature.

Although the mathematical model that includes the energy balance is a realistic model to simulate the reactor, from the experimental investigation of the oxidative dehydrogenation of ethane by Tonkovich *et al.,* (1996a), it was found that the radial dispersion had an effect on the inert membrane reactor. Higher temperature was observed near the membrane wall, where oxygen permeated into the catalyst bed. Yang *et al.,* (1998) studied the partial oxidation of methane to formaldehyde in the inert membrane reactor by doing both experiment and modeling. The model included the radial dispersion effect. The non-isothermal effect was ignored as they studied the reaction at low conversion range and, as a result, the increase of reaction temperature was small. The results from the mathematical simulation for the inert membrane reactor agreed with the experimental data over the range of operating conditions. However, no distinct improvement on selectivity to the desired product was obtained when a microporous oxide membrane was used.

CHAPTER III
THEORY

A membrane is an interface between two bulk phases. It controls the exchange of mass with differing chemical and physical properties between them. The membrane phase can be one or a combination of the following: a nonporous solid, microporous or macroporous solid with a fluid in the pores, a liquid phases with or without a second phase. The exchange between the two bulk phases across the membrane is caused from the presence of a driving force. The most common one is chemical potential such as pressure and concentration gradients and electrical potential.

A membrane reactor is an integration of two unit operations, i.e. reaction and separation (by a membrane), into a single one. It offers advantages not only in terms of system simplification but also yield improvement and selectivity enhancement. This new technology uses the membrane as a catalysts or a catalyst support and, at the same time, as a physical means for separating reactants and products by a controlled addition of a very active reactant or selective removal of undesirable intermediate reaction product to increase yield and selectivity. However, there are still several significant challenges that need to be addressed before the technology becomes both technically feasible and economically viable on a production scale.

There have been numerous studies exploring the concept of membrane reactors. Many of them, however, are related to biotechnological applications where enzymes are used as catalysts in many reactions such as hydrolysis of proteins at relatively low temperatures. Some applications such as production of monoclonal antibodies in a hollow fiber membrane bioreactor have just begun to be commercialized.

The greatest potentials of inorganic membranes are found on catalytic reactions. Many industrially significant reactions occur at high temperatures and often

under harsh chemical environments where inorganic membranes generally are the only choice of materials due to their inherent thermal and chemical stabilities. Commercialization of inorganic membranes, especially ceramic membranes, in recent years has spurred widespread interest not only in separation applications but also more importantly in membrane reactor applications and has generated a surge in the studies of inorganic membrane reactors.

In this chapter, the basic knowledge on inorganic membranes is provided as it is an important component of membrane reactor. The characteristics of gas removal and addition through the porous inorganic membrane can be illustrated by the transport mechanism. The concept of membrane reactor including the application areas is described. Finally the mechanism of oxidative dehydrogenation of *n*-butane on V/MgO is present.

3.1 Types of inorganic membranes

Table 3.1 classifies inorganic membranes according to their nature and to their most important characteristics: selectivity and permeability. Both are determined by the interaction between the membrane and the permeating molecules which result in different transport mechanisms.

Table 3.1 Classification of inorganic membranes.

Type of membrane	Material	Selectivity	Permeability
Dense	Metallic	High (H_2, O_2)	Low to moderate
	Solid electrolytes		
Porous (oxides, carbon, glass, metal, zeolites)			
	Macroporous	Non-selective	High
	Mesoporous	Low to moderate	Moderate to high
	Microporous	Can be very selective	Moderate
Composite	Glass-metal	Can be very selective	Moderate
	Ceramic-metal		
	Metal-metal		

3.1.1 Dense membrane (non-porous membrane)

Palladium and its alloys with ruthenium, nickel or other metals from group VI to VIII, silver, zirconia are examples of dense membranes. Dense membranes offer the highest selectivities or permselectivity for specific gases (e.g. H_2 and O_2) via transport processes that involve solution-diffusion or ionic conductivity mechanism. In return, permeation fluxes through selective, defect-free dense membranes are low and proportional to the thickness.

3.1.2 Porous membrane

Porous membranes can be made from various materials, such as ceramics, graphite, metal or metal oxides, and zeolites. Generally, the Porous membranes are not highly permselective. All gas species can permeate through the membrane at different rate. The mechanisms of gas transport through the porous membrane include viscous flow, Knudsen diffusion, surface diffusion, capillary condensation, and molecular sieving. These membranes are characterized by high permeability but low selectivity.

The porous membrane structure may be symmetric, i.e. the pore diameters do not vary over the membrane cross section, or they can be asymmetrically structured, e.g., the pore diameters increase from one side of the membrane to the other by a factor of 10 to 1,000.

The most important membrane used today for membrane reactor application has a rather sophisticated asymmetric structure. In this membrane, the two basic properties required of any membrane, e.g. high mass transport rates for certain components and good mechanical strength, are physically separated. An asymmetric membrane consists of a very thin (0.1 to 10 μm) selective skin layer (γ-alumina, zirconia, silica, etc.) on a highly porous (1 to 2 mm) thick substructure (generally α-alumina). The very thin skin represents the actual membrane. Its separation characteristics are determined by the nature of membrane and the pore size while the mass transport rate is determined by the membrane thickness, since the mass transport rate is inversely proportional to the thickness of the actual barrier layer. The porous

sublayer serves only as a support for the thin and fragile skin and has little effect on separation characteristics or the mass transfer rate of the membrane.

3.1.3   Composite membrane

Since the permeation fluxes of gas through defect-free dense membranes are low, the composite membranes are attempted to obtain simultaneously moderately high fluxes and high selectivities. In most cases, membranes consist of several layers with a pore size reduction in each layer. The membranes are called composite membranes. A porous substrate with a low resistance to permeation is covered with a thin dense membrane layer, which provides the desired selectivity. The porous substrates such as ceramic, metal, and glass supports seem to be the more preferable than other materials due to their excellent thermal and mechanical stability.
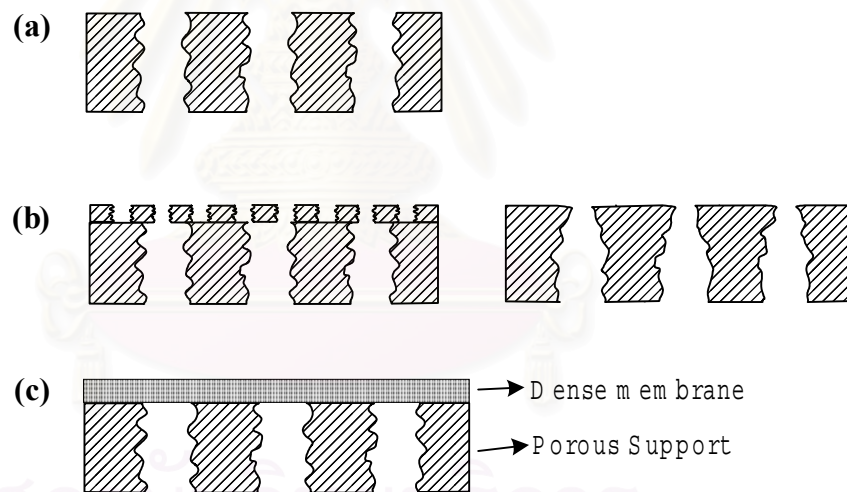
Figure 3.1 Schematic diagram of a (a) symmetric, (b) asymmetric and (c) composite membrane.

3.2 Classification of inorganic membrane reactors

The catalytic reactors based on ceramic membrane can be classified by the activation of membrane in the followings:

3.2.1   Inert membrane reactor (IMR)

In this type of reactor the catalytic material does not form part of the membrane. A typical configuration is a tubular membrane enclosing a fixed-bed of catalyst. In addition, the membrane does not participate in the reaction directly but it is used to add or remove certain species from the reactor. So the membrane is not damaged by the reaction such as coke deposition.

3.2.2   Catalytic membrane reactor (CMR)

In this case, the membrane participates in the reaction directly. The reaction appears at the surface or in the pores of membrane. The membrane material itself is catalytically active, or become active during preparation by the addition of active precursors. The advantage of these types is to solve the problem of diffusion resistance in catalyst pellet.

3.3 Transport mechanisms through porous inorganic membrane

Gas permeation across porous membrane can be described by five flow mechanisms: viscous bulk flow, Knudsen flow, surface diffusion, capillary condensation and molecular sieving, as shown in Figure 3.2. However, in practice only one or a few mechanisms predominate the total transport. This depends on the factors such as membrane pore size, molecule weight of permeants, interaction between gases and membrane, and operating conditions. Details of each gas permeation on mechanism are as follows.
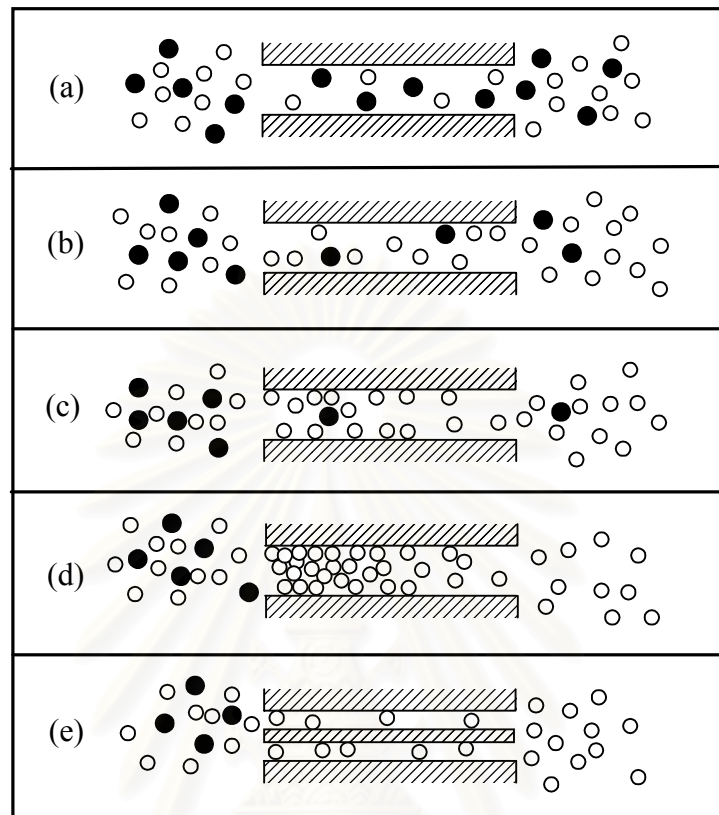
Figure 3.2 Transport mechanisms of gases mixtures through a porous membrane: (a) viscous flow; (b) Knudsen diffusion; (c) surface diffusion; (d) capillary condensation; and (f) molecular sieving (Saracco and Specchia, 1994).

3.3.1   Viscous bulk flow

Viscous bulk flow (or Poiseuille flow) takes place when the membrane pores are larger than the mean free paths of the permeating gas molecules. Momentum is exchanged among gas molecules during the collision. As a result, all molecules pass the pores with the average velocity independent of their sizes, shape or masses. This transport mechanism is non-separative.

For a porous membrane consisting of cylindrical capillary pores of equal size, the transport rate can be described by the Hagen-Poiseuille equation.

$$J_V = -\frac{\pi n d_{p,m}^4 P}{128 \tau_g \mu R_{gas} T}\frac{dP}{dz}$$

Where J_v is molar flux due to the viscous flow, n is the number of pores per unit area, $d_{p,m}$ is the pore diameter, P is the pressure, R_{gas} is the gas constant, T is the operating temperature, μ is gas viscosity, τ_g is the tortuosity of the pores for gas phase flow and z is the distance across the membrane. in reality, the pore structure in membranes are very complicated and frequently not known. Thus there are many factors introduced, for example average pore diameter, porosity, pore size distribution, tortuosity and specific surface area.

3.3.2 Knudsen diffusion

Knudsen flow regime occurs when membrane pore diameters are smaller than the mean free path of the gases to be separated. The collision frequency among gas molecules is negligible, compared with that of the gas molecules on the pore walls. Thus, each molecule passes the pore at its own molecular speed which is roughly inversely proportional to the square root of its molecular mass. This transport mechanism is separative, however, the selectivity of separation in this regime is not high. The Knudsen flux through porous membrane is given by

$$J_K = -\left(\frac{\pi n d_{p,m}^3}{12 R_{gas} T \tau_g}\sqrt{\frac{8 R_{gas} T}{\pi M}} \right)\frac{dP}{dz}$$

In this expression, J_k is the molar flux contributed by Knudsen flow and M is the molecular weight of the permeating gas.

3.3.3 Surface diffusion

This phenomena occurs when there exists an interaction between gases and pore walls. The gases are adsorbed as a film on the pore surface, and the migration of this adsorbed film causes an extra flow moving parallel to the bulk gas flow. In particularly, the surface flow is high at low temperature and high pressure. In the separation of a gas mixture, some gases are preferentially adsorbed on the pore surface while the other gases are not. These effects can be very significant in some

cases. As such the gases have very similar molecular weights, so can not be separated by Knudsen diffusion.

3.3.4   Capillary condensation

Capillary condensation takes place in porous membranes when the temperature decreases and/or the pressure of the adsorbable gas increases. The adsorbed phase in both monolayer and multilayer are gradually replaced by the capillary condensed phase. Transport in capillary condensation can be regarded as Poiseuille flow of a viscous liquid filling the pores of the porous media. When capillary condensation occurs, the passage of the nonadsorbed gas is reduced or totally blocked by the condensate filling the pores. Thus the more condensible gas can be separated from the less condensible one therefore the selectivity is usually high.

3.3.5   Molecular sieving

When the pore size of the membrane approaches the size of the molecule that is passing through it, a sieving mechanism can occur for gas separation. Selectivity based on this mechanism is very high because the separation is caused by size selection. The smaller molecules in a gas mixture are allowed to pass through the membrane while the larger molecules are obstructed.

3.3.6   Gas phase flow through alumina membrane

Because the temperature of gas phase oxidative dehydrogenation reaction is very high, over 773 K, the gas molecules are unlikely to be adsorbed on the membrane pore surface. The membranes used in this study have pore size of 4 nm. As a result, gas phase flow is the combination of Knudsen diffusion and viscous bulk flow and for the flux of a pure component, J, can be described by the combination of the expressions as follows

$$J = -\left(\frac{\pi n d_{p,m}^{3}}{12 R_{gas} T \tau_{g}} \sqrt{\frac{8 R_{gas} T}{\pi M}} + \frac{\pi n d_{p,m}^{4} P}{128 \tau_{g} \mu R_{gas} T} \right) \frac{dP}{dr}$$

where r is radial distance along the membrane.

Gases involved in oxidative dehydrogenation reaction is a gas mixture. Thus the molar flow rate of permeate gas per unit membrane length of component i $(F_i/L)'$ can be expressed as (Assabumrungrat and White, 1996)

$$\left(\frac{F_i}{L}\right)' = \left(\frac{a}{\sqrt{M_iT}}\left(P_1y_{i,1} - P_2y_{i,2}\right) + \frac{by_{i,1}}{2\mu T}\left(P_1^2 - P_2^2\right)\right)$$

$y_{i,1}$ and $y_{i,2}$ are mole fraction of species i in feed side and permeate side respectively.

3.4 Concepts of membrane reactor

In chemical processes, operating temperature of gas phase reactions is usually high. The use of inorganic membrane is necessary. The major advantages of membrane reactor are for improving reactor performance and energy management and reducing intensity of operating condition. The following sections provide details of the membrane reactor by dividing into 2 subsections according to the types of application of the membrane reactor.

3.4.1   Yield-enhancement of equilibrium-limited reactions

The most common application opportunity of membrane reactor lies in the circumvention of a chemical equilibrium so as to achieve higher per-pass conversions by selective permeation, through the membrane, of at least one of the reaction products. Most often, the removal of hydrogen in dehydrogenation reactions has been the process of choice and also been applied to other processes such as decomposition (H_2S, H_2O) and production of synthesis gas as shown in Figure 3.3a. Product removal may be selective (i.e., H_2 permeation through a composite Pd-ceramic membrane), or preferential (i.e., preferential permeation of H_2 versus higher molecular weight products using a Knudsen-diffusion membrane).

Equilibrium displacement can be enhanced through reaction coupling. Figure 3.3b shows the coupling of reactions at the opposite side of the membrane. In this case, on both sides of the membrane complementary processes are run using either the permeated species (chemical coupling, e.g., dehydrogenation/hydrogenation, or

dehydrogenation/combustion reactions), or the heat generated in the reaction (thermal coupling, exothermic/endothermic processes). The reactions often use different catalysts, which would be packed on opposite sides of the membrane tube.

The general case study for such application of inorganic membrane reactors is dehydrogenations. Since these reactions are endothermic, conversion is favored at high temperatures at the price of significant occurrence of side reactions, which reduce selectivity and lead to catalyst deactivation by coking. By using a membrane reactor, the same level of conversions could be obtained at lower temperatures thereby suppressing undesired reactions. Further, since dehydrogenations imply an increase of the overall number of gas molecules of the system, they can be forced to high conversions by reducing the operating pressure, which entails comparatively high reactor volumes. Such volumes could be reduced using a membrane reactor.
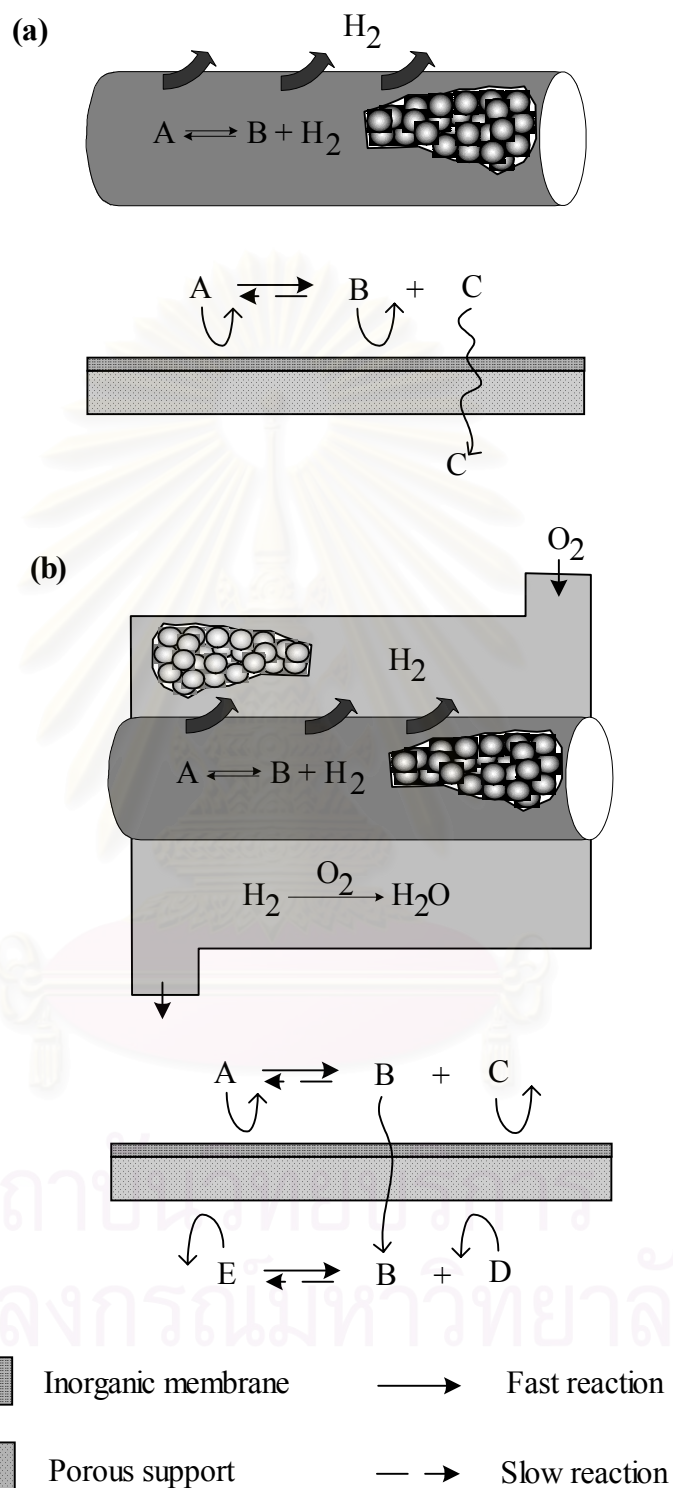
Figure 3.3 Application opportunities of inorganic membrane reactor (yield enhancement): (a) selective permeation of a reaction product of an equilibrium limited reaction; (b) coupling of reactions.

3.4.2   Selectivity enhancement

The improvement of reaction selectivity is a second field of application of membrane reactor on which most attention of the scientific community is nowadays addressed. In this context, considering consecutive reaction pathways, a permselective membrane could allow permeation of an intermediate product while rejecting either reactants or other undesired products as shown in Figure 3.4a. However, intermediate products (e.g. partially oxidized hydrocarbons) are larger than the complete reaction products (e.g. CO_2) or the reactants themselves (e.g. O_2). This requires the imaginative use of some unconventional permeation mechanisms (e.g. capillary condensation, surface diffusion or multi-layer diffusion), which is rather complex and strongly depends on the particular reaction and membrane considered. For such a reason no interesting practical applications of this concept are known.

Another opportunity for the increase of the reaction selectivity lies in the controlled addition of a reactant along the reactor, through either a permselective or non-permselective membrane as shown in Figure 3.4b. The most frequent case corresponds to a series-parallel reacting network where there is a favorable kinetic effect regarding the partial pressure of the distributed reactant. Thus, it has often been found in selective oxidation processes whose low partial pressure of oxygen favors the selective oxidation reaction versus the deep oxidation to CO and CO_2. Since oxygen is a necessary reactant, its presence in the reaction environment cannot be completely avoided, but its partial pressure can be lowered by distributing it through a porous membrane. Inert membrane reactors have been used successfully as oxygen distributors in a number of oxidation including methane oxidative coupling and the production of olefins and oxygenates from the oxidation of alkanes.

In general, the use of a membrane for the distribution of oxygen in oxidation processes produces not only greater selectivities with respect to conventional feed arrangements, but also a safer operation with reduced formation of hot spots and a lower probability of runaway. The avoidance of hot spots can give additional increments of selectivity by suppressing undesired reactions that take place at high temperatures, and in any case help to extend catalyst life. The distribution of oxygen

also allows a wider range of operating conditions: by distributing the oxygen feed in the inert membrane reactor it is possible to operate at overall hydrocarbon to oxygen ratios that would be within the explosive region if the same composition was fed at the entrance of a fixed-bed reactor.
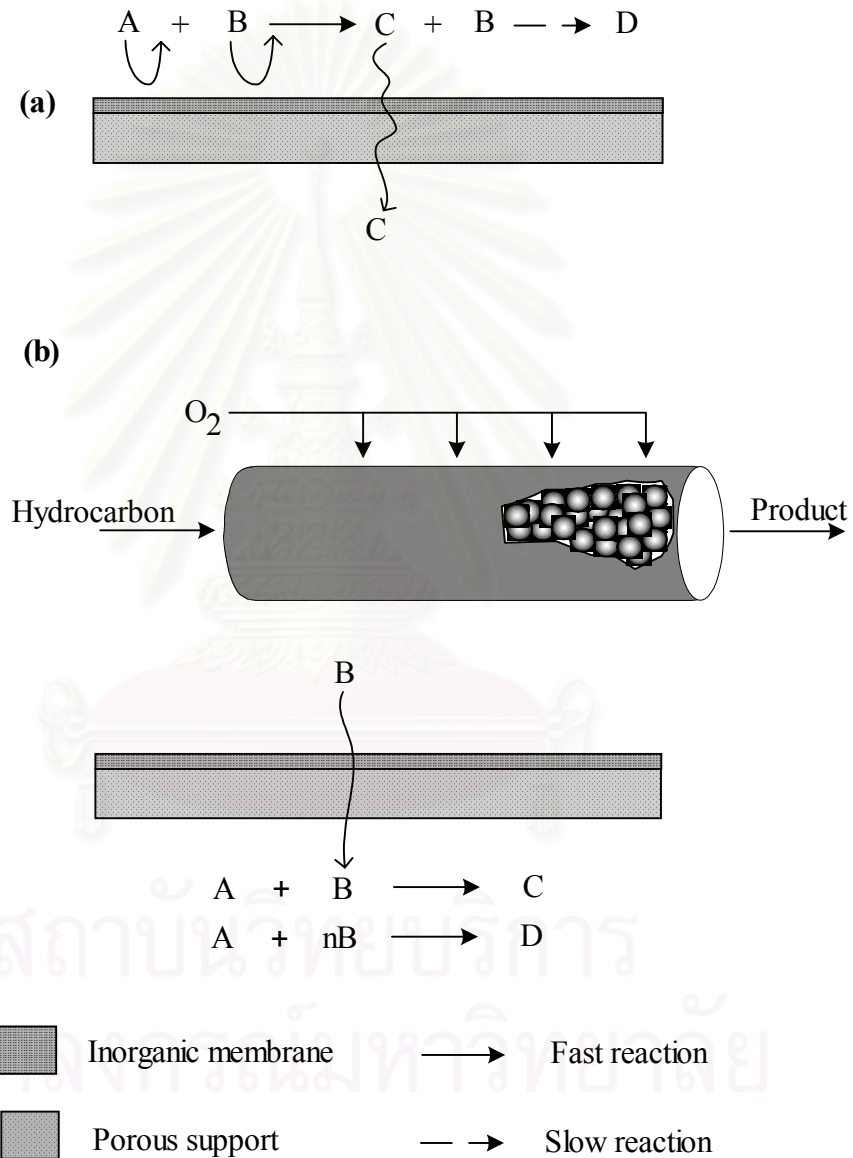
Figure 3.4 Application opportunities of inorganic membrane reactor
(selectivity enhancement): (a) selective permeation of an intermediate, desired product; (b) dosing a reactant through the membrane.

3.5 Oxidative dehydrogenation of *n*-butane

The oxidative dehydrogenation of *n*-butane to butene and butadiene accompanied by side reactions of deep oxidation of products and reactant to CO and CO_2. The reaction networks of oxidative dehydrogenation of *n*-butane on V/MgO (Tellez *et al*., 1999b) are shown in Figure 3.5. Reactions 1,2 and 3 in this scheme refer, respectively, to the formation of 1-butene, cis-2-butene and trans-2-butene from butane. The C_4H_8 in reaction 7, 8 and 9 includes the lumped reaction of 1-butene, trans-2-butene and cis-2-butene.
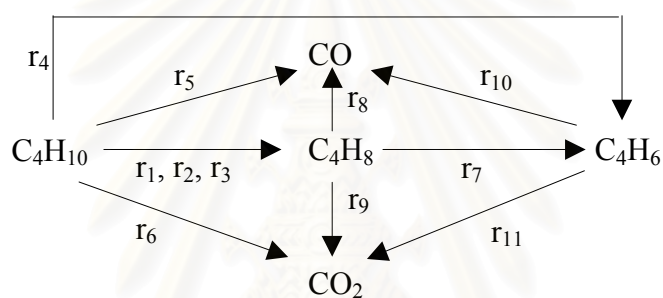
Figure 3.5 The reaction network of *n*-butane oxidative dehydrogenation.

CHAPTER IV
MATHEMATICAL MODEL

The membrane reactor in this study is a double tubular reactor; the inner tube is made of an γ-Al$_2$O$_3$ inorganic membrane, and the outer shell of a stainless steel. The membrane is composite in nature. The separation layer is made from γ-Al$_2$O$_3$ with pore diameter of 4 nm and thickness of 5μm, the detail is described in Table 4.1. The V/MgO catalyst (24wt% of V$_2$O$_5$) is packed in the shell side where a mixture of nitrogen and n-butane is introduced. Air is fed into the tube side. For a fixed-bed reactor, the feed is a mixture of nitrogen, *n*-butane and air. The kinetic data by Tellez et al., 1999b was used in the simulation (shown in Appendix A). The gas permeation through the membrane is based on the permeation data of gases through a commercial "Membralox" membrane (Assabumrungrat and White, 1996). The expression for gas permeation rate of component *i* per unit length of the membrane $(F_i/L)'$ is shown in Equation 4.1.

$$\left(\frac{F_i}{L}\right)' = \frac{a(P_t y_{i,t} - P_s y_{i,s})}{\sqrt{M_i T}} + \frac{b y_{i,t}(P_t^2 - P_s^2)}{2\mu T} \tag{4.1}$$

a and b are Knudsen and viscous flow parameters, respectively. $y_{i,t}$ and $y_{i,s}$ are mole fractions of species *i* in tube side and shell side respectively.

Table 4.1 Characteristics of a membrane.

Support Composition	α - alumina
Membrane Composition	γ - alumina
Membrane Pore Size (m)	4×10^{-9}
Separative Thickness (m)	5×10^{-6}
Internal Diameter (m)	0.007
Outside Diameter (m)	0.010

Pseudo-homogeneous models for the case with and without radial effect were developed using the following assumptions:

1. Steady-state condition
2. The ideal behavior of gases can be used to determine gas properties.
3. The pressure is constant at both the shell and tube side, neglecting pressure drop.
4. The temperature at the reactor wall is constant and equal to a coolant.
5. Axial dispersion of mass and heat are neglected.
6. The interfacial mass transfer resistance between the gas and the surface of membrane is small compared with the internal mass transfer resistance in the membrane.
7. The membrane is catalytically inactive.
8. The inert membrane reactor is operated in co-current mode.

Details of the development of fixed-bed reactor and inert membrane reactor models are given in Appendix D. For a plug flow model the 4th order Runge-Kutta method was employed to integrate the differential equations while a finite differential method was used for the radial diffusion model. The followings summarize the sets of equations for both reactors and both models.

4.1 Fixed-bed reactor (FBR)

4.1.1 Plug flow model

Mole balances of species i

$$\frac{d\overline{F_i}}{d\overline{Z}} = \frac{\rho_B A_C L}{F_{T,0}} r_i \tag{4.2}$$

Energy balance

$$\sum \left(\overline{F_i} C_{pi}\right)\frac{d\overline{T}}{d\overline{Z}} = \frac{U_{SS} A_P}{F_{T,0}} \left(\overline{T_j} - \overline{T}\right) + \frac{A_C L \rho_B}{F_{T,0} T_0} \sum \left(R_i \left(-\Delta H_{ri}\right)\right) \tag{4.3}$$

4.1.2 Radial diffusion model

Mole balances of species *i*

$$\frac{\partial \overline{F_i}}{\partial \overline{Z}} = \alpha_{FBR}\left[\frac{1}{R}\frac{\partial}{\partial R}\left(\frac{\overline{F_i}}{\overline{F_T}\,\overline{T}}\right) + \frac{\partial^2}{\partial R^2}\left(\frac{\overline{F_i}}{\overline{F_T}\,\overline{T}}\right)\right] + \frac{A_C L \rho_B}{F_{T,0}} r_i \qquad (4.4)$$

$$\overline{Z} = 0 ; \qquad \overline{F_i} = \overline{F_{i,0}} \qquad (0 < R < 1)$$

$$R = 0 ; \qquad \frac{\partial}{\partial R}\left(\frac{\overline{F_i}}{\overline{F_T}\,\overline{T}}\right) = 0$$

$$R = 1 ; \qquad \frac{\partial}{\partial R}\left(\frac{\overline{F_i}}{\overline{F_T}\,\overline{T}}\right) = 0$$

Energy balance

$$\frac{\partial \overline{T}}{\partial \overline{Z}} = \beta_{FBR}\left[\frac{1}{R}\frac{\partial \overline{T}}{\partial R} + \frac{\partial^2 \overline{T}}{\partial R^2}\right] + \frac{\rho_B A_C L}{F_{T,0}T_0\left(\sum C_{Pi}\overline{F_i}\right)}\sum\left(R_i\left(-\Delta H_{ri}\right)\right) \qquad (4.5)$$

$$\overline{Z} = 0 ; \qquad \overline{T} = 1$$

$$R = 0 ; \qquad \frac{\partial \overline{T}}{\partial R} = 0$$

$$R = 1 ; \qquad -\frac{2\pi L \lambda_{er}}{A_P}\frac{\partial \overline{T}}{\partial R} = U_{SS}\left(\overline{T}_{R=1} - \overline{T_j}\right)$$

4.2 Inert membrane reactor (IMR)

4.2.1 Plug flow model

Mole balances of species *i*

Shell side:

$$\frac{d\overline{F_i^s}}{d\overline{Z}} = \frac{\rho_B A_{Cs} L}{F_{T,0}^s} r_i + \frac{L}{F_{T,0}^s}\left(\frac{F_i}{L}\right)' \qquad (4.6)$$

          rate of reaction   permeation

Tube side:

$$\frac{d\overline{F_i^t}}{d\overline{Z}} = -\frac{L}{F_{T,0}^t}\left(\frac{F_i}{L}\right)'$$

(4.7)

Energy balance

Shell side:

$$\sum\left(\overline{F_i^s}C_{pi}\right)\frac{d\overline{T_s}}{d\overline{Z}} = \frac{U_{SS}A_{P3}}{F_{T,0}^s}(\overline{T_j} - \overline{T_s}) - \frac{U_M A_{P1}}{F_{T,0}^s}(\overline{T_s} - \gamma_1\overline{T_t})$$

<div align="center">heat transfer through heat transfer through
stainless steel   membrane</div>

$$+ \sum\frac{L}{F_{T,0}^s T_{s,0}}\left(\frac{F_i}{L}\right)' H_i + \frac{A_{Cs}L}{F_{T,0}^s T_{s,0}}\rho_B\sum\left(R_i(-\Delta H_{ri})\right)$$

(4.8)

<div align="center">heat transfer by   heat of reaction
mass permeation</div>

Tube side:

$$\sum\left(\overline{F_i^t}C_{pi}\right)\frac{d\overline{T_t}}{d\overline{Z}} = \frac{U_{SS}A_{P1}}{F_{T,0}^t}(\gamma_2\overline{T_s} - \overline{T_t}) + \sum\frac{L}{F_{T,0}^t T_{t,0}}\left(\frac{F_i}{L}\right)' H_i$$

(4.9)

4.2.2   Radial diffusion model

Mole balances of species *i*

Shell side:

$$\frac{\partial\overline{F_i^s}}{\partial\overline{Z}} = \alpha_{IMR,s}\left[\frac{1}{(R_s + R_2)}\frac{\partial}{\partial R_s}\left(\frac{\overline{F_i^s}}{F_T^s\overline{T_s}}\right) + \frac{\partial^2}{\partial R_s^2}\left(\frac{\overline{F_i^s}}{F_T^s\overline{T_s}}\right)\right]$$

(4.10)

$$+ \frac{A_{Cs}L\rho_B}{F_{T,0}}r_i$$

$$\overline{Z} = 0 ; \qquad \overline{F_i^s} = \overline{F_{i,0}^s} \qquad (0<R_s<1)$$

$$R_s = 0 \, ; \qquad -D_{er}^s \frac{P_s}{R_{gas} T_{s,0}} \frac{d}{dR_s}\left(\frac{\overline{F_i^s}}{\overline{F_T^s}\,\overline{T_s}} \right) = \frac{L}{A_{P2}}\left(\frac{F_i}{L} \right)'$$

$$R_s = 1 \, ; \qquad \frac{\partial}{\partial R_s}\left(\frac{\overline{F_i^s}}{\overline{F_T^s}\,\overline{T_s}} \right) = 0$$

Energy balance

Shell side:

$$\frac{\partial \overline{T_s}}{\partial \overline{Z}} = \beta_{IMR,s}\left[\left(\frac{1}{R_s + R_2} \right)\frac{\partial \overline{T_s}}{\partial R_s} + \frac{\partial^2 \overline{T_s}}{\partial R_s^{\,2}} \right] + \frac{\rho_B A_{Cs} L}{F_{T,0}^s T_{s,0}\left(\sum C_{Pi}\overline{F_i^s} \right)}\sum\left(R_i\left(-\Delta H_{ri} \right) \right) \quad (4.11)$$

$$\overline{Z} = 0; \qquad \overline{T_s} = 1$$

$$R_s = 0 \, ;$$

$$-\frac{\pi \lambda_{er}^s}{A_{Cs}} \frac{\partial \overline{T_s}}{\partial R_s} = U_M\left(\gamma_1 \overline{T_t}_{\,R_t=1} - \overline{T_s}_{\,R_s=0} \right) + \sum \frac{L}{A_{P2}T_{s,0}}\left(\frac{F_i}{L} \right)' H_i$$

$$R_s = 1 \, ; \qquad -\frac{\pi \lambda_{er}^s}{A_{Cs}} \frac{\partial \overline{T_s}}{\partial R_s} = U_{SS}\left(\overline{T_s}_{\,R_s=1} - \overline{T_j} \right)$$

It is noted that the plug flow condition was assumed for the flow in the tube side (oxygen feed side). The expressions for the mass balance and the energy balance are the same and the plug flow model as given in Equations 4.7 and 4.9, respectively.

CHAPTER V
RESULTS AND DISCUSSION

Two mathematical models of plug flow model and radial diffusion model were developed to investigate performance of fixed-bed reactors and membrane reactors. For the fixed-bed reactor (FBR) gas mixture of n-butane, air and N_2 was fed to the catalyst bed while for the inert membrane reactor (IMR) air was fed to the tube side whereas n-butane and N_2 was fed to the catalyst bed in the shell side. In this chapter the effect of operating variables and design parameters on performance of oxidative dehydrogenation of n-butane in both reactor types was presented. The standard operating condition and reactor configuration used in this study for both fixed-bed reactor and inert membrane reactors are given in Table 5.1 and 5.2 respectively. Deviation from the values will be stated as appropriate.

Table 5.1 The standard reactor configuration.

Type of reactor	I.D. (m)	O.D. (m)
Fixed-bed reactor	0.006	0.009
Inert membrane reactor		
Tube side (membrane tube)	0.007	0.01
Shell side (stainless steel)	0.0117	0.0147

Table 5.2 The standard condition and range of parameter in study.

Parameters	Standard condition	Value in study
Total molar flow rate (mol/s)	4.464×10^{-4}	4.464×10^{-4}
Inert introgen flow rate (mol/s)	2.976×10^{-4}	2.976×10^{-4}
Reactant flow rate (mol/s)	1.488×10^{-4}	1.488×10^{-4}
Air to n-butane ratio in reactant feed	8	1-15
Pressure (kPa)	101.3	101.3
Feed temperature (K)	773	773
Coolant temperature (K)	773	753-803
Catalyst size (μm)	250	250
Packed bed density (kg/m^3)	700	700
Packed bed porosity	0.5	0.5
Reactor diameter (m)	0.006	0.006-0.05
a, Knudsen parameter ($\frac{mol \times K^{1/2}}{m \times s \times kPa}$)	4.8×10^{-3}	4.8×10^{-3}
b, Viscous parameter ($\frac{mol \times K}{m \times kPa}$)	1×10^{-12}	1×10^{-12}

5.1 Performance of fixed-bed reactor

5.1.1   Effect of reaction temperature
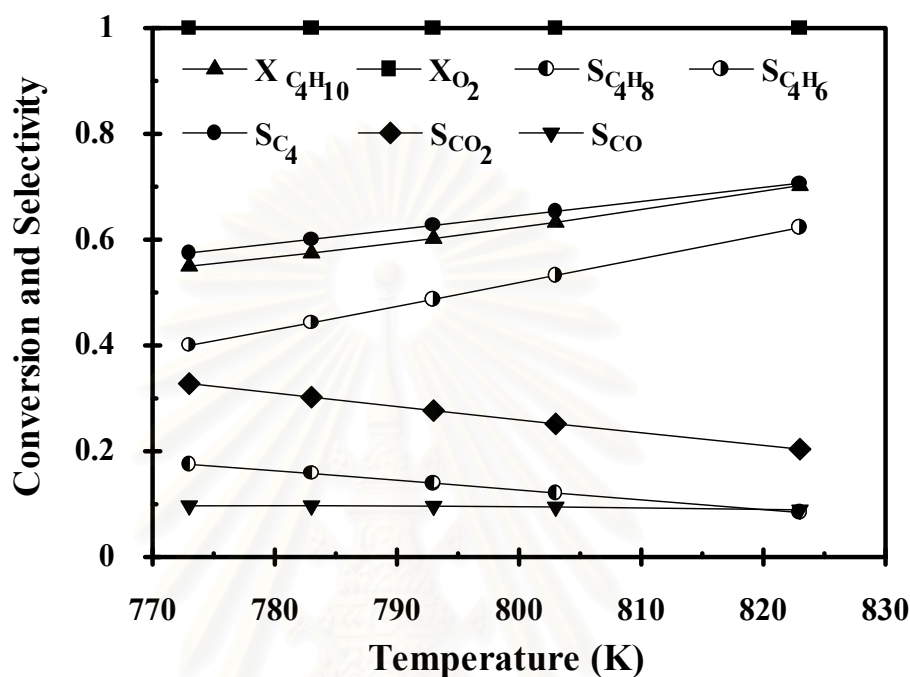
Figure 5.1 Effect of reaction temperature (Isothermal plug flow model, air/*n*-butane ratio 8, d = 0.006 m, feed flow rate of *n*-butane 1.65×10^{-5} mol/s, T_f and T_j = 773 K, $W/F_{C_4H_{10},0}$ = 160 kg s/mol)

Figure 5.1 shows the performance of the fixed-bed reactor at various operating temperature. The conversion of *n*-butane and oxygen and selectivity to butene, butadiene, total dehydrogenated C_4 products (summation value of the selectivity to butene and butadiene), carbon dioxide and carbon monoxide were presented. The increase of the reaction temperature increases the conversion of *n*-butane but decreases the selectivity to carbon dioxide and butene. The selectivity to carbon monoxide is almost constant. However, the selectivity to butadiene is more favorable at high temperature than the selectivity to butene, resulting in the increased selectivity to the total dehydrogenated C_4 products. It can be concluded that the desired products C_4 are favorable at high operating temperature. All of these trends agree with previously published experimental results (Tellez *et al.,* 1997 and Lemonidou *et al.,* 1998).

5.1.2   Comparison between plug flow model and radial model

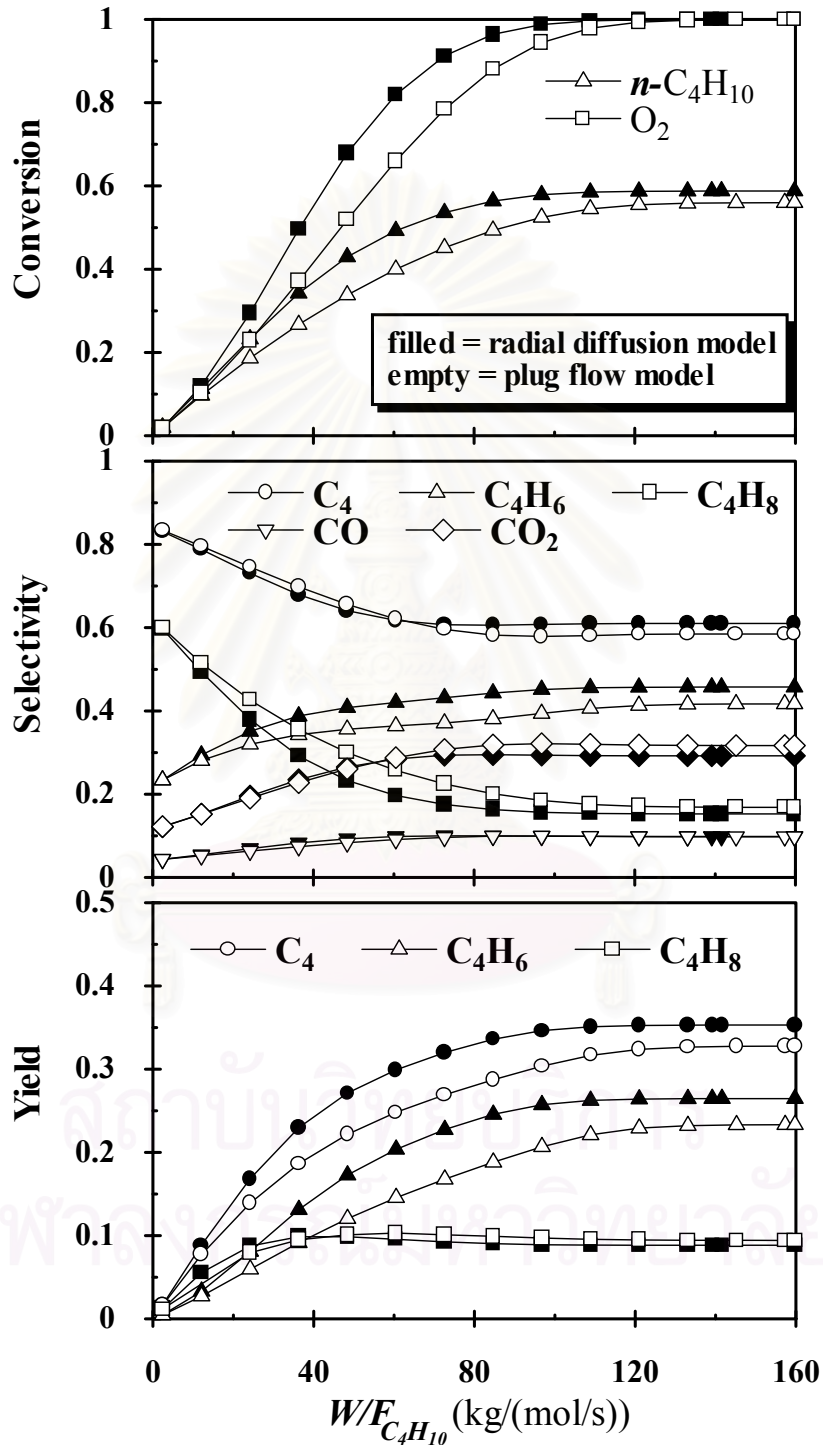**Figure 5.2** Conversion, selectivity and yield of plug flow and radial diffusion model (air/*n*-butane ratio 8, d = 0.006 m, feed flow rate of *n*-butane 1.653×10^{-5} mol/s, T_f and T_j = 773 K)

Figure 5.2 compares the results of the fixed-bed reactor between two models; i.e. the model without radial dispersion (plug flow model) and the model taking into account radial dispersion (radial model). The filled symbols show the values from the radial model while the empty symbols show the values from the plug flow model. $W/F_{C_4H_{10}}$ denotes the catalyst weight divided by the molar flow rate of butane. It was found that when $W/F_{C_4H_{10}}$ increases the conversion of n-butane and oxygen increases while the selectivity to butene decreases and reaches the asymptote. On the contrary, the selectivity to butadiene and carbon oxides shows opposite results. This is because butene is a primary reaction product while butadiene and carbon oxides are both primary and secondary reaction products. The comparison between the filled symbols and the empty symbols shows that the radial dispersion effect is pronounced. This effect can be seen more clearly in Figures 5.3 and 5.4. Because the oxidative dehydrogenation is a highly exothermic reaction and the reactions take place mainly near the entrance of the reactor, the hot spot where the temperature reaches the maximum value can be found. The hot spot temperature from the plug flow model differs significantly from the average temperature from the radial model. As a result, the conversion of reactant and selectivity to total dehydrogenation C_4 product was higher in the radial diffusion model due to the higher temperature. Figure 5.4 emphasizes that the rate of heat removal from the reactor center to the wall was slow due to the presence of radial heat dispersion. As a result, the temperature difference between the reactor center and the wall was high. Hence, the following studies will be carried out using the radial model.
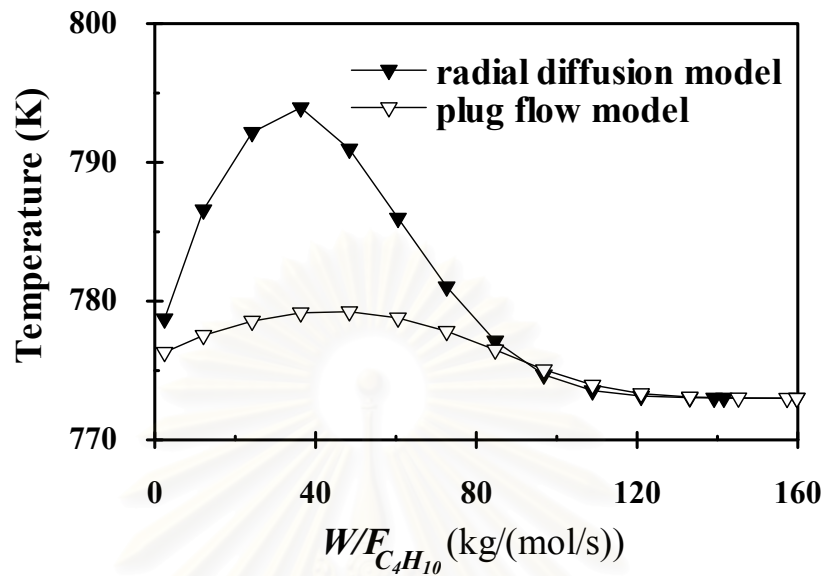
Figure 5.3 Temperature profile of plug flow and radial diffusion model (air/*n*-butane ratio 8, d = 0.006 m, feed flow rate of *n*-butane 1.653×10^{-5} mol/s, T_f and T_j = 773 K)
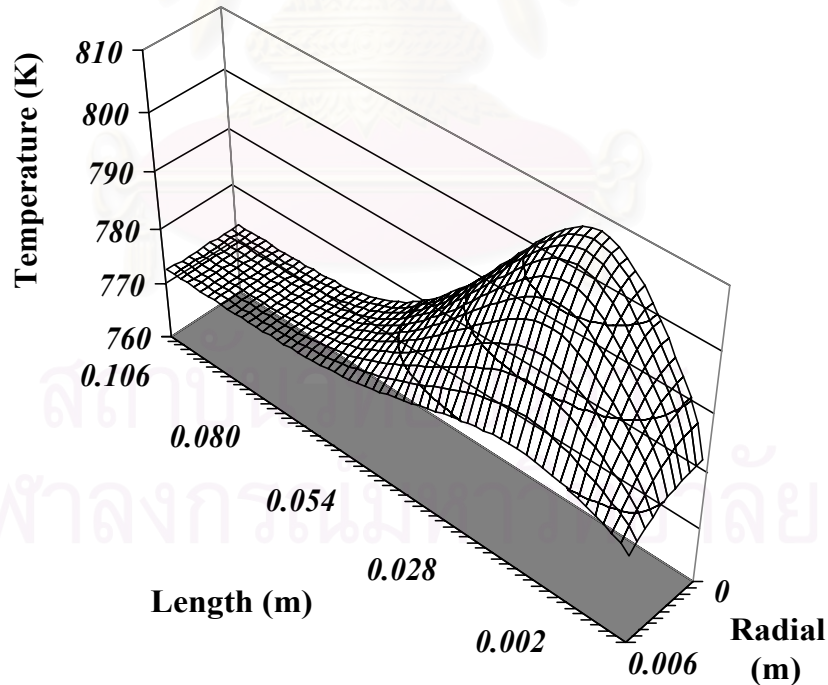
Figure 5.4 Temperature profile in radial diffusion model (air/*n*-butane ratio 8, d = 0.006 m, L = 0.24 m, feed flow rate of *n*-butane 1.653×10^{-5} mol/s, T_f and T_j = 773 K, $W/F_{C_4H_{10}}$ = 150 kg s/mol)

5.2 Membrane reactor study

<u>5.2.1 Comparison between fixed-bed reactor and membrane reactor</u>
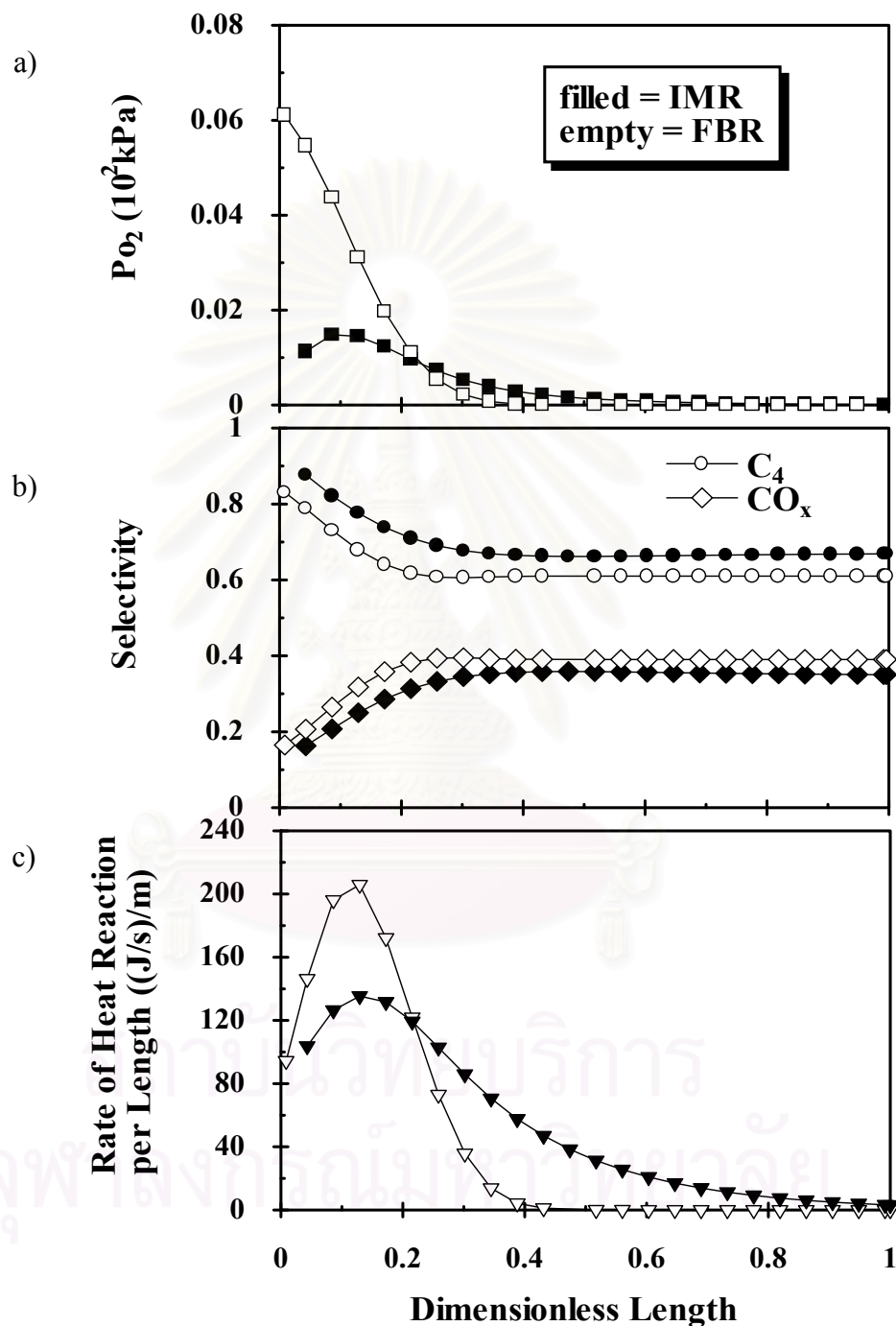
Figure 5.5 Comparison of FBR and IMR. a) partial pressure of oxygen in catalyst bed. b) selectivity. c) heat of reaction (air/*n*-butane ratio 8, d = 0.006 m, L = 0.24 m, feed flow rate of *n*-butane 1.653×10^{-5} mol/s, T_f and T_j = 773 K)

Figure 5.5 compares the results of the fixed-bed reactor and membrane reactor. It is obvious that the partial pressure of oxygen along the reactor length for the membrane reactor is smoother than that of the fixed-bed reactor. This is because the membrane was employed to distribute oxygen to the reaction chamber along the reactor length. The results also show one advantage on the selectivity improvement by using the controlled addition of oxygen to keep the partial pressure of oxygen at low value. As a result, complete oxidation to CO and CO_2 was suppressed. This phenomena was also found in other system such as oxidative coupling of methane (Lafarga *et al.,* 1994b). Another point to be addressed is that due to lower amount of O_2 at the entrance the heat of reaction for the membrane reactor is less severe than the fixed-bed reactor.

5.2.2   Effect of air to *n*-butane ratio

Figure 5.6 compares the performance of the fixed-bed reactor and membrane reactor at various ratio of air to *n*-butane flow rate. It can be seen that the increase of the ratio results in the increased conversion and decreased selectivity. At low value of the ratio, on the other words lower amount of oxygen, the conversion and selectivity for both reactors are almost the same. However, when the ratio increases the selectivity to the total dehydrogenated C_4 products of the membrane reactor becomes superior to the fixed-bed reactor. In this study, it was found that there is an optimum ratio where the yield to the total dehydrogenated C_4 is maximum, the ratio of 8 for the fixed-bed reactor and 9 for the membrane reactor. At low value of the ratio even though the selectivity is high but the conversion is low as the amount of oxygen is limited; however, at very high value of the ratio the reaction products are oxidized to form carbon oxides. It should be noted that another important advantage of the membrane reactor is on the avoidance of hot spot as found in the figure that the hot spot temperature of the fixed-bed reactor is much higher than that of the membrane reactor which is independent of the feed ratio.
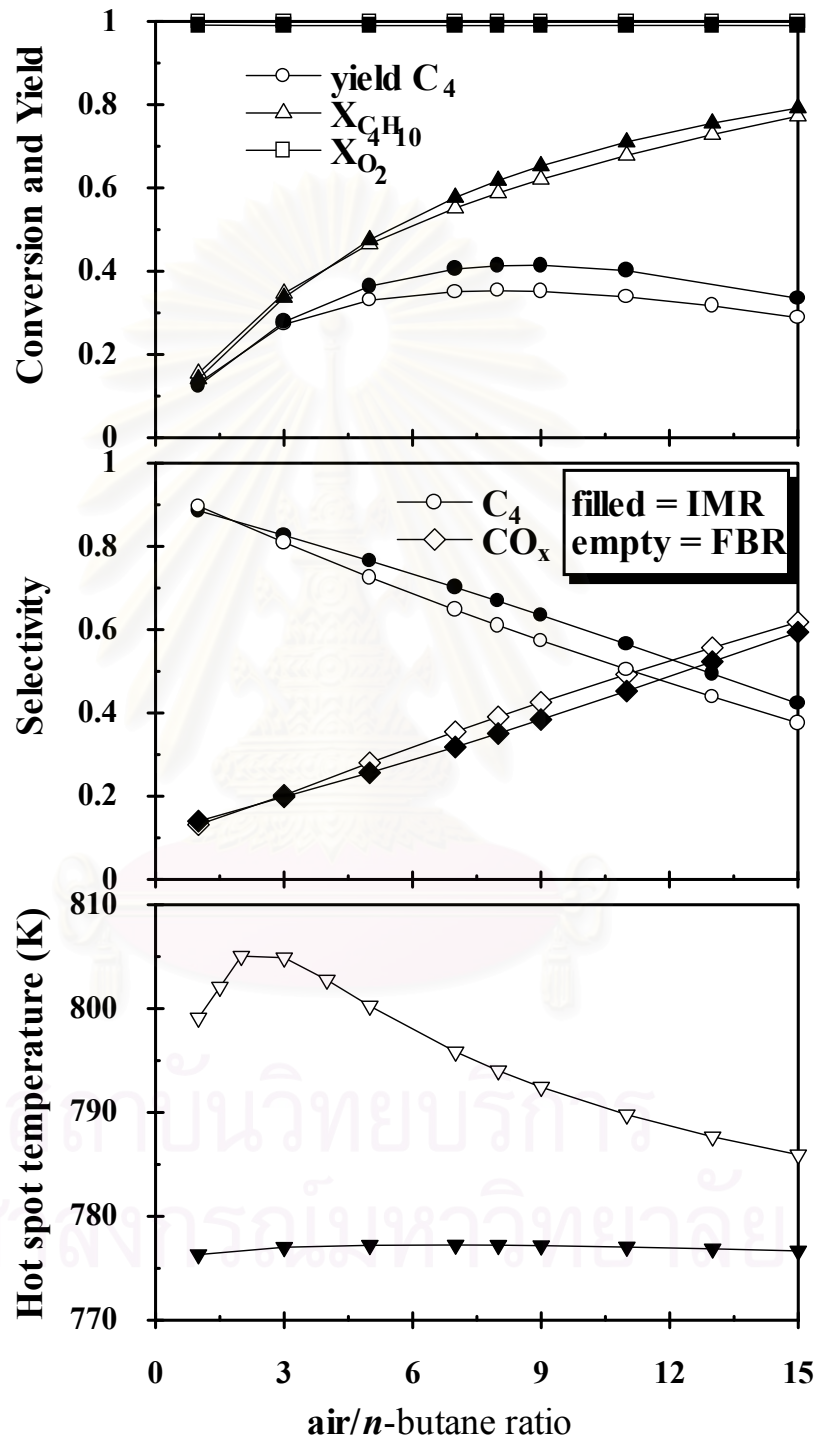
Figure 5.6 Effect of the air/*n*-butane ratio to performance of reactor (d = 0.006 m, T_f and T_j = 773 K, L = 0.24 m)

5.2.3   Effect of reactor diameter
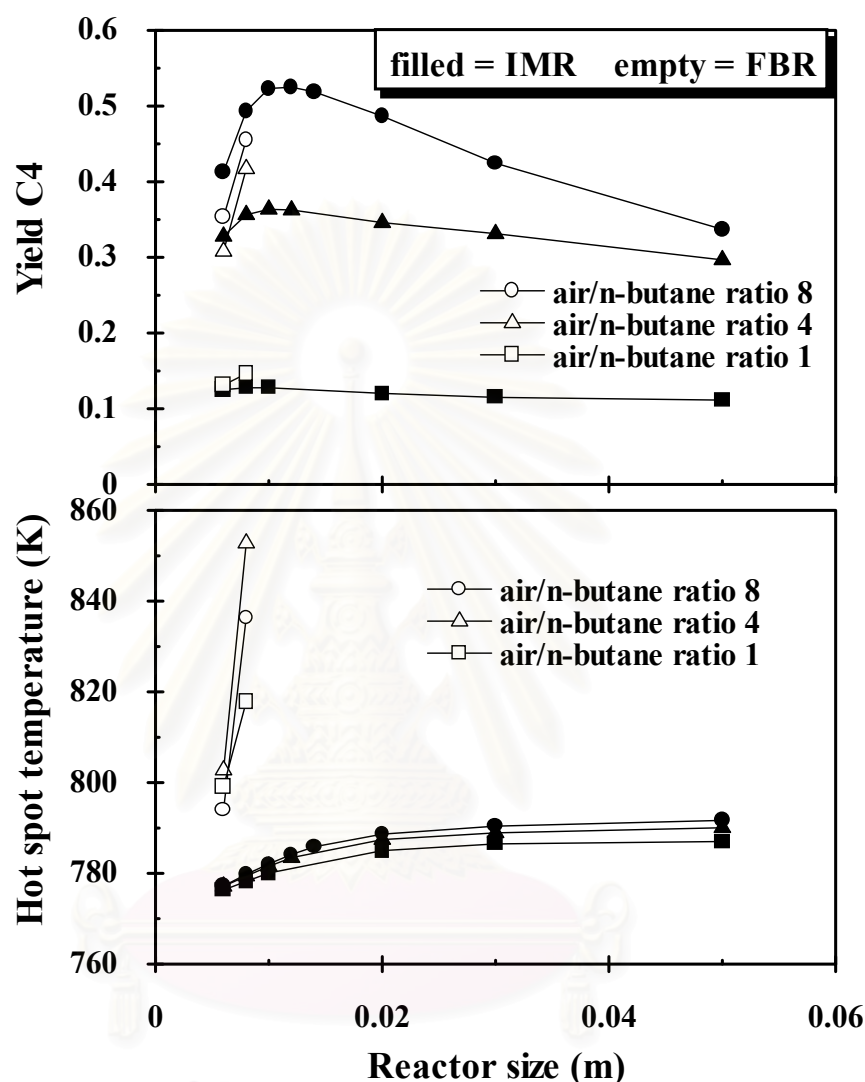
Figure 5.7 Effect of reactor diameter on yield C4 and hot spot temperature (air/*n*-butane ratio of 1,4 and 8, T_f and T_j = 773 K, L = 0.24 m)

Figure 5.7 shows the effect of the reactor size to the performance of the reactors. The specification of the reactor at different size is summarized in Table 5.3. The increase of the reactor size while keeping the membrane surface area constant results in the increased amount of catalyst for the reaction; however, it is expected that the effect of radial dispersion should be more pronounced. It was found that for the fixed-bed reactors at various feed ratios the increase of reactor size significantly

Table 5.3 The reactor size in study.

Reactor size	Fixed-bed reactor		Membrane reactor	
	I.D. (m)	O.D. (m)	I.D. (m)	O.D. (m)
0.006	0.006	0.009	0.0117	0.0147
0.01	0.01	0.013	0.0141	0.0171
0.02	0.02	0.023	0.0224	0.0254
0.03	0.03	0.033	0.0316	0.0346
0.05	0.05	0.053	0.051	0.054

Note: The reactor size of inert membrane reactor was calculated based on the equivalent area of the reaction zone.

increases the hot spot temperature while relatively small increase of the hot spot temperature was observed in the membrane reactor. One interesting results found in this study is that there is an optimum reactor diameter where the yield of total dehydrogenated product C_4 is maximum. The optimum reactor diameter equal to 0.012, 0.01 and 0.008 m for membrane reactor at air/*n*-butane ratio of 8, 4 and 1 respectively while an optimum reactor diameter was not found for the fixed-bed reactors. The presence of optimum reactor size for the membrane reactor can be described by considering Figures 5.8 and 5.9.
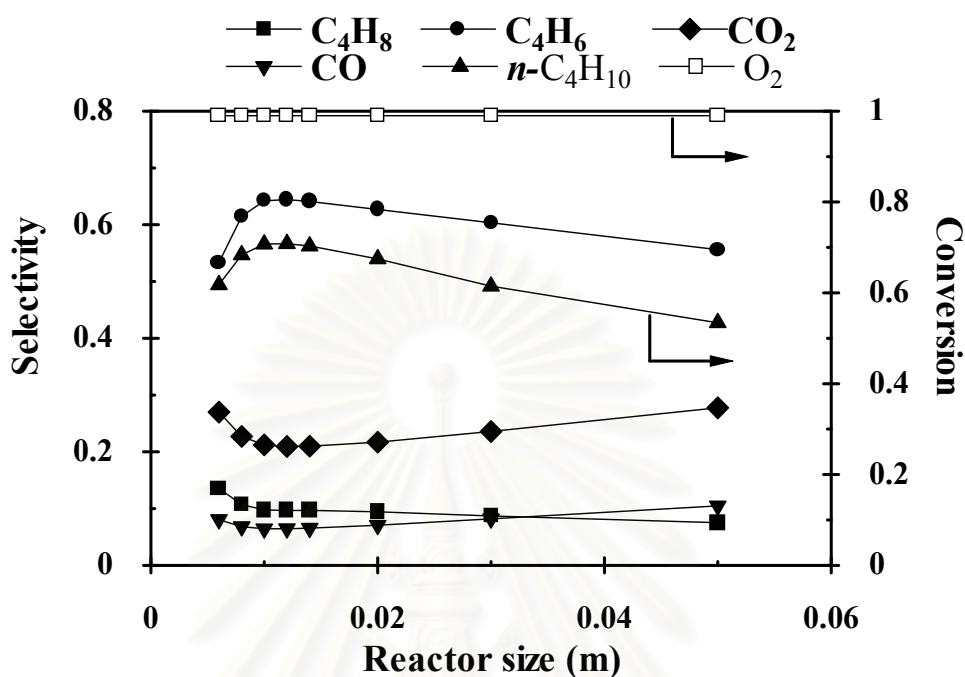
Figure 5.8 Effect of reactor diameter on selectivity and conversion (air/*n*-butane ratio 8, feed flow rate of *n*-butane 1.653×10^{-5} mol/s, T_f and T_j = 773 K, L = 0.24 m)

In Figure 5.8 the conversion and the selectivity are shown for the case where the air/*n*-butane ratio is equal to 8. It was found that the oxygen conversion is 100% for all the reactor sizes. From the optimum value of the reactor size, when the reactor size increases, the conversion of *n*-butane decreases. It means that oxygen was consumed to oxidize the product to carbon oxides as found that the selectivity to butadiene and butene decreases while the selectivity to carbon dioxide and carbon monoxide increases. This can be explained that oxygen fed from the tube side can not reach *n*-butane near the shell wall due to the effect of radial dispersion as shown in Figure 5.9 that the partial pressure difference of *n*-butane at the stainless steel surface and the membrane surface for the reactor size of 0.05 m is much higher than that of 0.012 m. When the reactor size decreases, the extent of reaction decreases due to the smaller amount of catalyst. As a result, the yield decreases.

In addition, Figure 5.9 shows the radial effect at different reactor size. The increase of reactor size increases the radial dispersion effect. However, the partial pressure of oxygen shows the opposite trend because the oxygen is consumed at higher reaction rate due to the increased volume of catalyst. The radial heat effect was also found to be more significant for larger reactor size.

Figure 5.9 Effect of reactor size to partial pressure and temperature along the reactor (air/*n*-butane ratio 8, feed flow rate of *n*-butane 1.653×10^{-5} mol/s, T_f and T_j = 773 K, L = 0.24 m)

5.2.4   Effect of reactor wall temperature
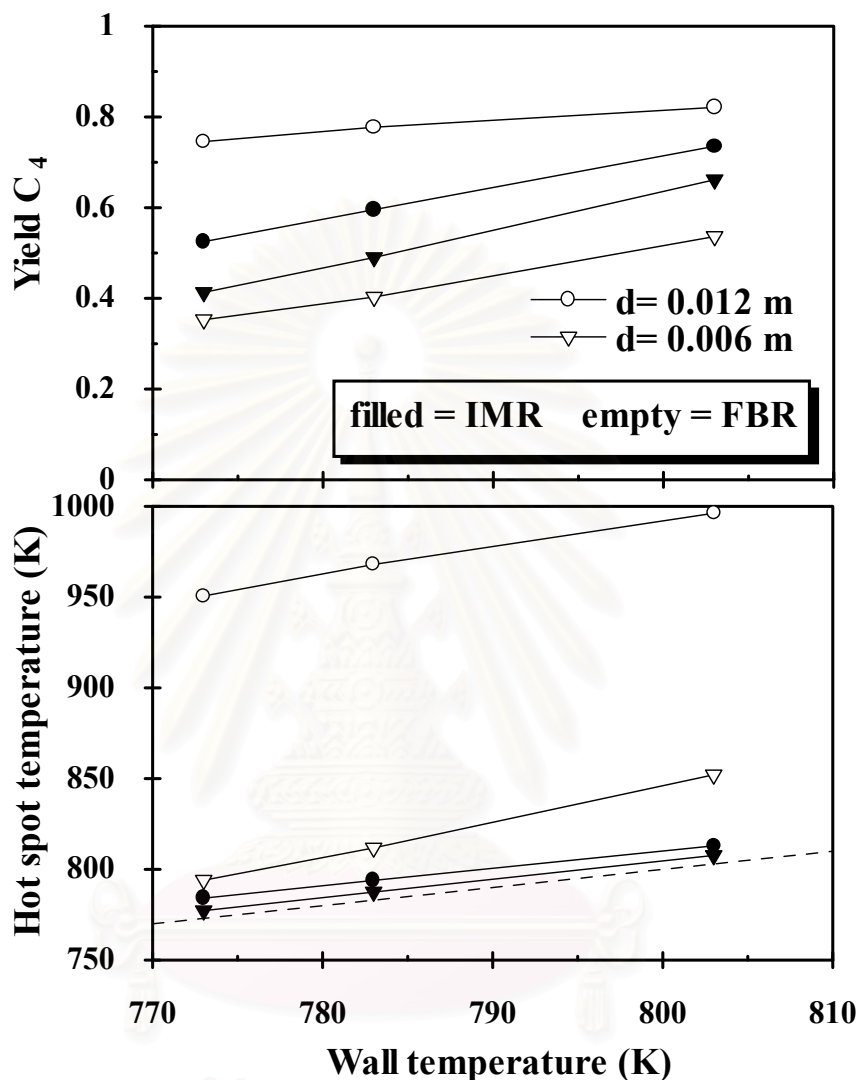
Figure 5.10 Effect of wall temperature to fixed-bed reactor and membrane reactor (air/*n*-butane ratio 8, feed flow rate of *n*-butane 1.653×10^{-5} mol/s, T_f = 773 K, d = 0.006 and 0.012 m, L = 0.24 m)

The effect of wall temperature was observed and the results are shown in Figure 5.10. With the increased wall temperature the yield of product C_4 becomes higher. For the fixed-bed reactor the increase of wall temperature significantly increases the hot spot temperature. Conversely, relatively small increase of the hot spot temperature was observed in the membrane reactor. The results are similar to the effect of reactor size. It should be noted that for the case of fixed-bed reactor with

reactor size of 0.012 m, the increase of wall temperature significantly enhance the yield, however, it leads to much higher hot spot temperature which should be avoided in practical operation.
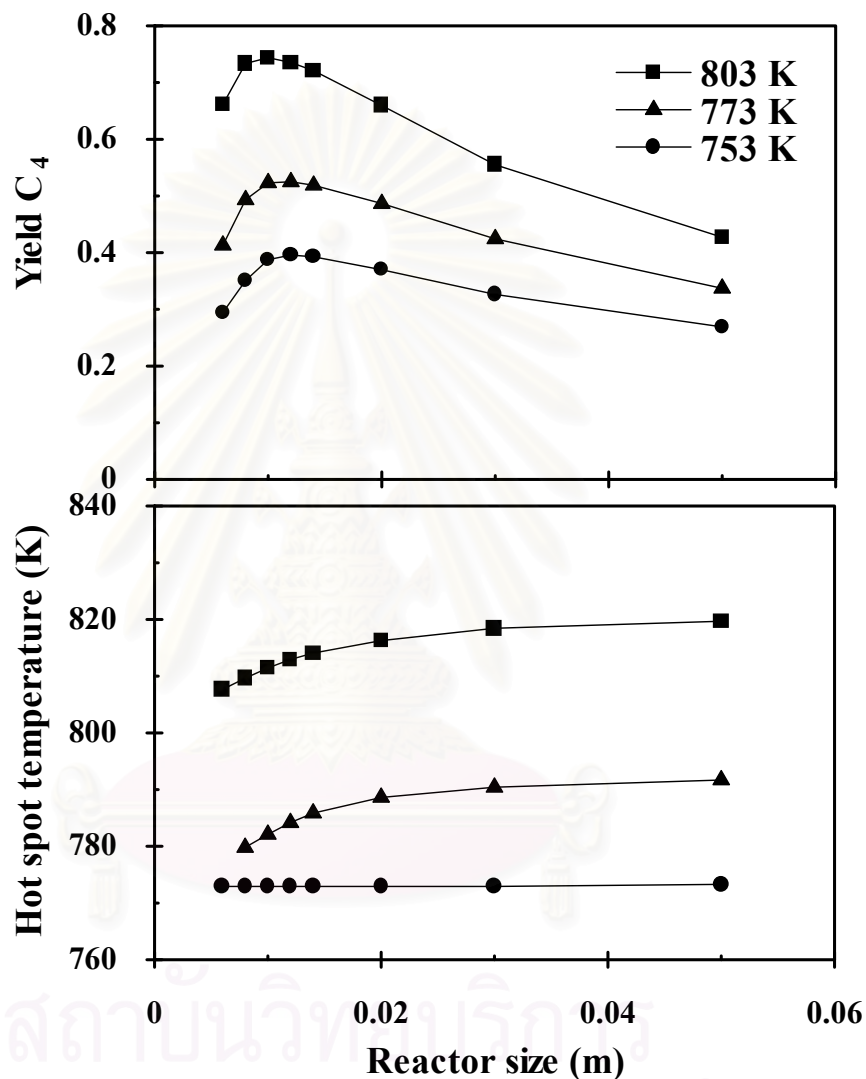
Figure 5.11 Effect of wall temperature to reactor size (air/*n*-butane ratio 8, feed flow rate of *n*-butane 1.653×10^{-5} mol/s, T_f = 773 K, L = 0.24 m)

Figure 5.11 emphasizes the effect of wall temperature. From the results it was found that at any wall temperature the optimal reactor size can be found. The optimal reactor sizes were 0.013, 0.012 and 0.01 m for the wall temperature of 753 K, 773 K and 803 K respectively. It is noted that the increase of wall temperature decreased the optimum reactor size. In addition, when the reactor size increased after the optimum

value, the yield C_4 of the high wall temperature case dropped faster than that of the low wall temperature case. This is because the increase of the wall temperature accelerates the effect of radial dispersion as shown in Figure 5.12. However, the partial pressure of oxygen shows the opposite way because oxygen was consumed at faster rate with higher temperature, as a result, partial pressure of oxygen at the membrane surface decreased with the increase of wall temperature.
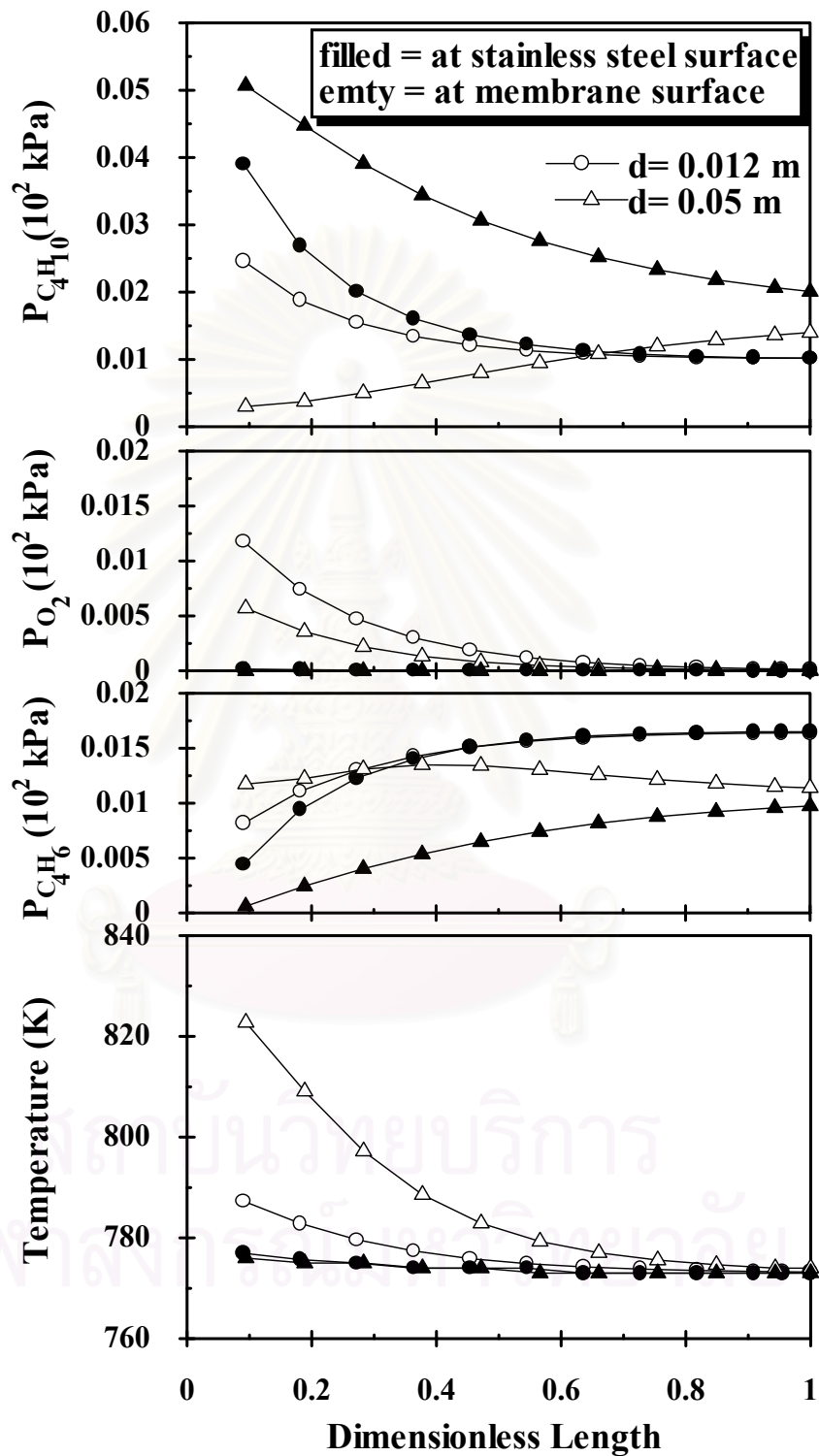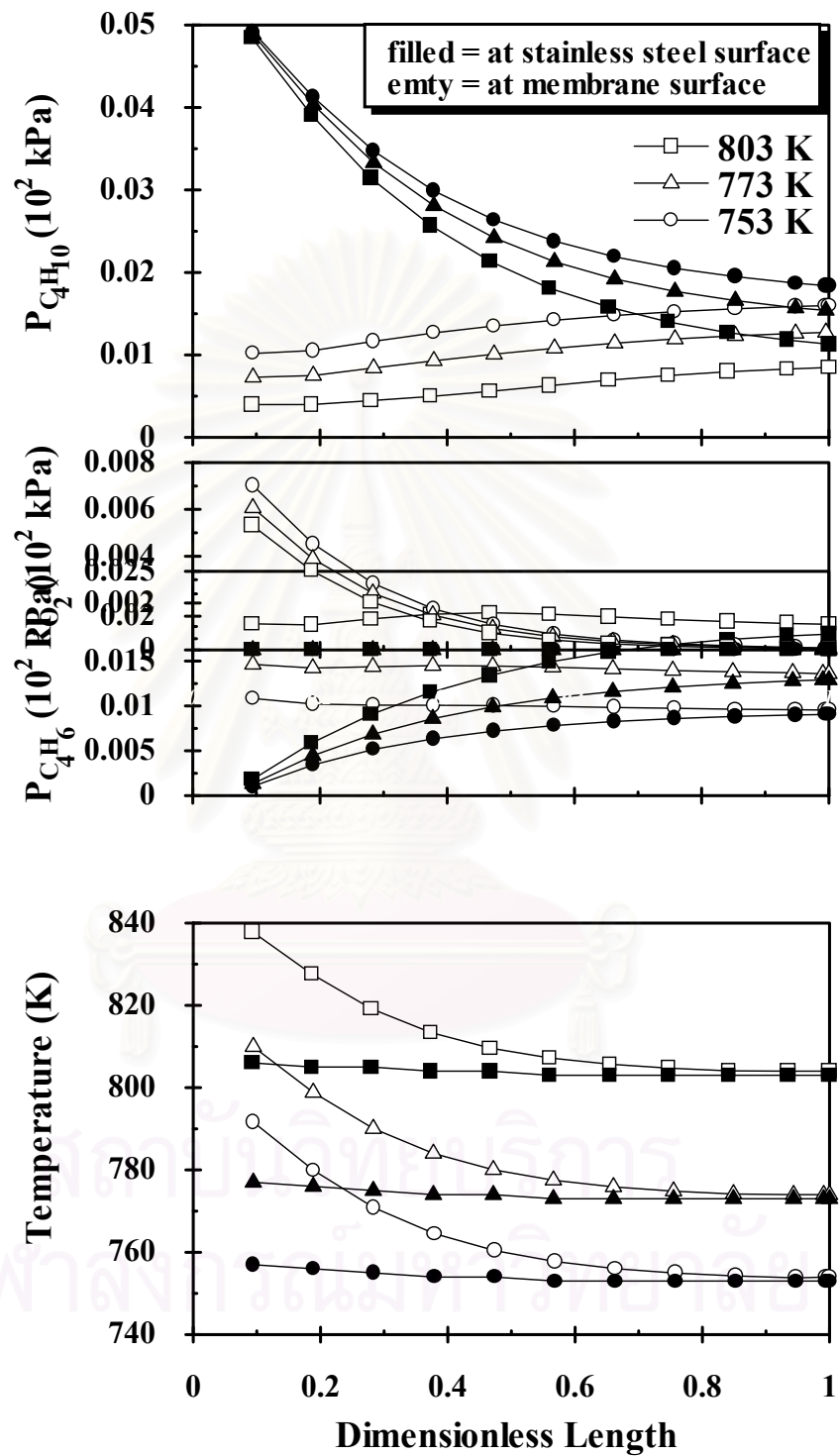
Figure 5.12 Effect of wall temperature to partial pressure and temperature a long the reactor (air/*n*-butane ratio 8, feed flow rate of *n*-butane 1.653×10^{-5} mol/s, T_f = 773 K, d = 0.03 m, L = 0.24 m)

5.2.5   Effect of feed air temperature
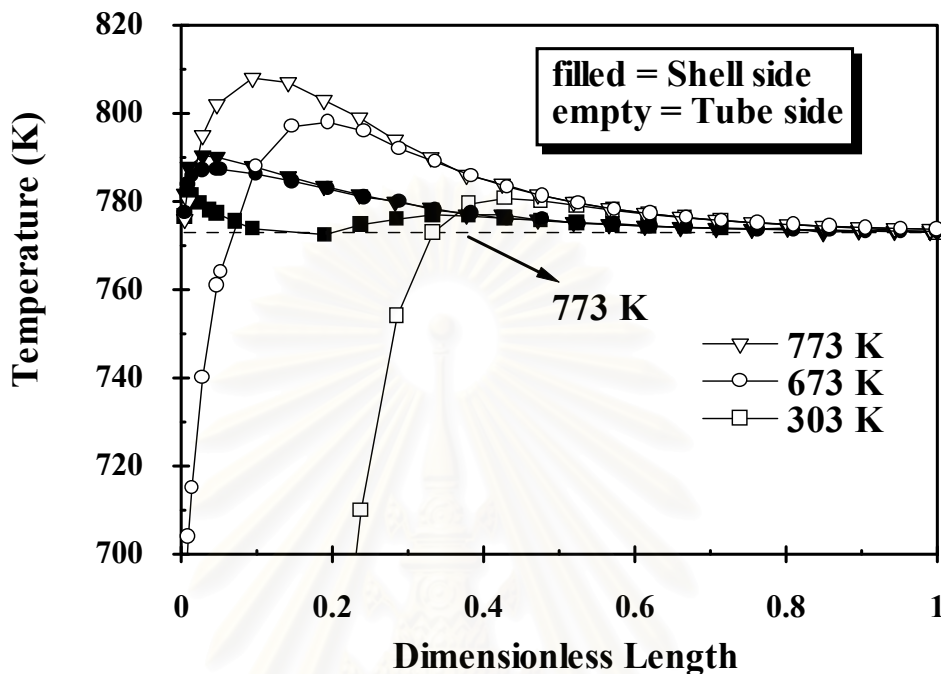
Figure 5.13 Effect of feed air temperature (air/*n*-butane ratio 8, feed flow rate of *n*-butane 1.653×10^{-5} mol/s, $T_{f,n\text{-}butane}$ = 773 K, T_j = 773 K, L = 0.24 m)

Figure 5.13 shows the effect of feed air temperature on the temperature profile along the reactor length. It is desirable to operate the reactor at small hot spot temperature to avoid subsequent problems such as catalyst deactivation and run-away reaction. It was found that the decrease of feed air temperature can reduce the hot spot temperature as the temperature profile became close to the isothermal condition. The heat of reaction which occurred mainly near the membrane surface can directly transfer to the cold feed air as found that the temperature in the tube side rapidly increased and reached to the asymtope.

CHAPTER VI
CONCLUSION AND RECOMMENDATION

The oxidative dehydrogenation of *n*-butane in the inert membrane reactor was studied. The ceramic membrane was used to add oxygen to the reaction side in a controlled manner so that the reaction can take place evenly. From the results, the following conditions can be addressed.

1. The selectivity to the C_4 hydrocarbon fovours at high operating temperature.
2. The effect of radial dispersion is significant especially where the hot spot takes place.
3. The membrane reactor outperforms the fixed-bed reactor in term of yield C_4 at high air/*n*-butane ratio or in the excess oxygen condition. In addition, the hot spot problem can be significantly improved using the membrane reactor.
4. For the membrane reactor there is the optimal reactor size for each of air/*n*-butane ratio. However, for the fixed-bed reactor the optimal size does not exist and the increase of reactor size the significantly increases in the hot spot temperature. The increase of reactor size accelerates the reaction with the expense of the more pronounced radial dispersion effect.
5. The increase of wall temperature increases the yield of C_4 hydrocarbon and radial dispersion effect.
6. The feed air temperature was found to be able to control the temperature profile along the reactor length

Recommendations

This work studied the oxidative dehydrogenation of *n*-butane in the ceramic membrane reactor by computer simulation. Although the membrane reactor outperformed the fixed-bed reactor by improving the selectivity and reducing the hot spot temperature, this study was limited to the condition where the pressure in both tube side and shell side was equal to 101.3 kPa. In the other words, no convection was assumed in the model. It is recommended to include the radial convection term in the model. It is believed that the use of high pressure in the feed air side can control the addition of O_2 to the system so that the reactor performance can be come better.

REFERENCES

Alfonso, M.J.; Julbe, A.; Farrusseng, D.; Menendez, M. and Santamaria, J. Oxidative dehydrogenation of propane on V/γ-Al$_2$O$_3$ catalytic membranes. Effect of the type of membrane and reactant feed configuration. Chem. Eng. Sci. 54 (1999): 1265-1272.

Alfonso, M.J.; Menendez, M. and Santamaria, J. Vanadium-based catalytic membrane reactors for the oxidative dehydrogenation of propane. Catal. Today 56 (2000): 247-252.

Al-Sherehy, F.A.; Adris, A.M.; Soliman, M.A. and Hughes, R. Avoidance of flammability and temperature runaway during oxidative dehydrogenation using a distributed feed. Chem. Eng. Sci. 53 (1998): 3965-3976.

Armor, N.J. Application of catalytic inorganic membrane reactors to refinery products. J. Memb. Sci. 147 (1998): 217-233.

Assabumrungrat, S. Mechanisms and modelling of gas separations through ceramic membranes in chemical reaction processes. Ph.D. Dissertation Imperial college of science, technology and medicine. (1996).

Barbieri, G. and P. Di Maio, F. Simulation of the methane steam re-forming process in a catalytic Pd-membrane reactor. Ind. Eng. Chem. Res. 36 (1997): 2121-2127.

Bernstein, L.A. and Lund, C.R.F. Membrane reactors for catalytic series and series-parallel reactions. J. Membrane Sci. 77 (1993): 155-164.

Blasco, T.; Lopez Nieto, J.M.; Dejoz, A. and Vazquez, M.I. Influence of the acid-base character of supported vanadium catalysts on their catalytic properties for the oxidative dehydrogenation of n-butane. J. Catal. 157 (1995): 271.

Capannelli, G.; Carosini, E.; Cavani, F.; Monticelli, O. and Trifiro, F. Comparison of the catalytic performance of V$_2$O$_5$/γ-Al$_2$O$_3$ in the oxidehydrogenation of propane to propylene in different reactor configuration: i) Packed-bed reactor, ii) Monolith-like reactor and iii) Catalytic membrane reactor. Chem. Eng. Sci. 51 (1996a): 1817-1826.

Capannelli, G.; Carosini, E. and Monticelli, O. Enhancement of the catalytic

performance of $V_2O_5/\gamma\text{-}Al_2O_3$ catalysts in the oxidehydrogenation of propane to propylene by the use of a monolith-type reactor. Catal. Lett. 39 (1996b): 241-246.

Carl L. Yaws Chemical properties handbook. (n.p.): McGraw-Hill, (1999).

Casanave, D.; Giroir-Fendler, A.; Sanchez, J.; Loutaty, R. and Dalmon, J.-A. Control of transport properties with a microporous membrane reactor to enhance yields in dehydrogenation reactions. Catal. Today 25 (1995): 309-314.

Casanave, D.; Ciavarella, P.; Fiaty, K. and Dalmon, J.-A. Zeolite membrane reactor for isobutane dehydrogenation: Experimental results and theoretical modeling. Chem. Eng. Sci. 54 (1999): 2807-2815.

Cheng, Y.S. and Yeung, K.L. Palladium-silver composite membranes by electroless plating technique. J. Membrane Sci. 158 (1999): 127-141.

Ciebien, J.F.; Cohen, R.E. and Duran, A. Membrane catalysts for partial hydrogenation of 1,3-butadiene: catalytic properties of palladium nanoclusters synthesized within diblock copolymer films. Material Sci. Eng. C7 (1999): 45-50.

Collins, J. and Way, J. Catalytic decomposition of ammonia in a membrane reactor. J. Membrane Sci. 96 (1994): 259-274.

Collins, J. and Brinker, C.J. Catalyst dehydrogenation in hydrogen permselective membrane reactor. Ind. Chem. Eng. Res. 35 (1996): 4398-4405.

Coronas, J.; Menendez, M. and Santamaria, J. Use of a ceramic membrane reactor for the oxidative dehydrogenation of ethane to ethylene and higher hydrocarbons. Ind. Eng. Chem. Res. 34 (1995a): 4229-4234.

Coronas, J.; Menendez, M. and Santamaria J. The porous-wall ceramic membrane reactor: an inherently safer contacting device for gas-phase oxidation of hydrocarbons. J. Loss. Prev. Process Ind. 8 (1995b): 97-101.

Dejoz, A.; Lopez Nieto, J.M.; Marquez, F. and Vazquez, M.I. The role of molybdenum in Mo-doped V-Mg-O catalysts during the oxidative dehydrogenation of n-butane. Appl. Catal. 180 (1999): 83-94.

Edlund, D.J. and Pledger, W.A. Catalytic platinum-based membrane reactor for removal of H_2S from natural gas streams. J. Membrane Sci. 94 (1994): 111-119.

Frank, P.I. and David, P. De Witt Fundamentals of heat and mass transfer. (n.p.): John Wiley & Sons, (1990).

Froment, G.F. and Bischoff, K.B. Chemical reactor analysis and design. (n.p.): John

Wiley & Sons, (1990).

Galuszka, J.; Pandey, R.N. and Ahmed, S. Methane conversion to syngas in a palladium membrane reactor. Catal. Today 46 (1998): 83-89.

Gobina, E.; Hou, K. and Hung, R. Mathematical analysis of ethylbenzene dehydrogenation comparison of microporous and dense membrane system. J. Memb. Sci. 105 (1995): 163-176.

Gobina, E. and Hughes, R. Reaction coupling in catalytic membrane reactors. Chem. Eng. Sci. 51 (1996): 3045-3050.

Gryaznov, V.M. and Slin'ko, M.G. Selectivity in catalysis by hydrogen-porous membranes. Discuss. Faraday. Soc. 72 (1982): 73-93.

Gryaznov, V.M. Hydrogen permeable palladium membrane catalysis. Plat. Met. Rev., 30 (1986): 68-72.

Gryaznov, V.M. Membrane catalysis. Catal. Today 51 (1999): 391-395.

Hermann, Ch.; Quicker, P. and Dittmeyer, R. Mathematical simulation of catalytic dehydrogenation of ethylbenzene to styrene in a composite palladium membrane reactor. J. Membrane Sci. 136 (1997): 161-172.

Incropera, F.P. and De Witt, D.P. Fundamentals of heat and mass transfer. (n.p.): John Wiley & Sons, (1990).

Itoh, N. A membrane reactor using Pd AIChE. J. 33 (1987): 1576-1580.

Itoh, N.; Xu, W.C. and Sathe, A.M. Capability of permeate hydrogen through Pd-base membranes for acetylene hydrogenation. Ind. Chem. Eng. Res. 32 (1993): 2614-2619.

Itoh, N,; Xu, W.C. and Haraya, K. Radial mixing diffusion of hydrogen in a packed-bed type of palladium membrane reactor. Ind. Eng. Chem. Res. 33 (1994): 197-202.

Itoh, N. and Wu, T.-H. An adiabatic type of palladium membrane reactor for coupling endothermic and exothermic reactions. J. Membrane Sci. 124 (1997): 213-222.

Kao, Y.K. A comparative simulation study on oxidative coupling of methane in fixed-bed and membrane reactor. Ind. Eng. Chem. Res. 36 (1997): 3583-3593.

Kikuchi, E. Palladium/ceramic membranes for selective hydrogen permeation and their application to membrane reactor. Catal. Today 25 (1995): 333-337.

Kikuchi, E. Membrane reactor application to hydrogen production. Catal. Today 56

(2000): 97-101.

Koukou, M.K.; Papayannakos, N. and Markatos, N.C. Dispersion effect on membrane reactor performance. <u>AIChE. J.</u> 42 (1996): 2607-2615.

Koukou, M.K.; Chaloulou, G.; Papayannakos, N. and Markatos, N.C. Mathematical modelling of the performance of non-isothermal membrane reactors. <u>Int. J. Heat Mass Transfer.</u> 40 (1997): 2407-2417.

Lafarga, D.; Santamaria, J. and Menendez, M. Methane oxidative coupling using porous ceramic membrane reactors I. Reactor development. <u>Chem. Eng. Sci.</u> 12 (1994a): 2005-2013.

Lafarga, D.; Santamaria, J. and Menendez, M. Methane oxidative coupling using porous ceramic membrane reactors II. Reaction studies. <u>Chem. Eng. Sci.</u> 12 (1994b): 2015-2025.

Lambert, C.K. and Gonzalez, R.D. Activity and selectivity of a Pd/Al_2O_3 catalyst membrane in the partial hydrogenation reaction of acetylene and 1,3-butadiene. <u>Cat. Letter.</u> 57 (1999): 1-7.

Lee, S.-J.; Yang, S.-M. and Park, S.B. Synthesis of palladium impregnated alumina membrane for hydrogen separation. <u>J. Membrane Sci.</u> 96 (1994): 223-232.

Lemonidou, A.A.; Tjatjopoulos, G.J. and Vasalos, I.A. Investigations on the oxidative dehydrogenation of n-butane over VMgO-type catalysts. <u>Catal. Today</u> 45 (1998): 65-71.

Li, S.; Jin, W.; Huang, P.; Xu, N. and Shi, J. Perovskite-related ZrO_2-doped $SrCo_{0.4}Fe_{0.6}O_{3-\delta}$ membrane for oxygen permeation. <u>AIChE. J.</u> 45 (1999): 276-284.

Liu, C.; Xu, Y.; Liao, S. and Yu, D. Mono- and bimetallic catalytic hollow-fiber reactors for the selective hydrogenation of butadiene in 1-butene. <u>Appl. Catal.</u> 172 (1998): 23-29.

Lu, Y.; Dixon, A.G.; Moser, W.R. amd Ma, Y.H. Analysis and optimization of cross-flow reactors for oxidative coupling of methane. <u>Ind. Eng. Chem. Res.</u> 36 (1997): 559-567.

Martin-Aranda, R.M.; Portela, M.F.; Madeira, L.M.; Freire, F.; and Oliveira, M. Effect of alkali metal promoters on nickel molybdate catalyst and its relevance to the selective oxidation of butane. <u>Appl. Catal.</u> 127 (1995): 201.

Miguel, M.P.; Coronas, J.; Menendez, M. and Santamaria, J. Methane oxidative

coupling over different alkali-doped catalysts: A comparison of ceramix membrane reactors and conventional fixed bed reactors. React. Kinet. Catal. Lett. 59 (1996): 277-284.

Mills, A.F. Basic heat and mass transfer. (n.p.): Richard D. Irwin, Inc., (1995).

Mleczko, L.; Ostrowski, T. and Wurzel, T. A fluidized-bed membrane reactor for the catalytic partial oxidation of methane to synthesis gas. Chem. Eng. Sci. 51 (1996): 3187-3192.

Nieto, J.M.L.; Dejoz, A.; O'Leary, W. and Cunningham, J. Oxidative dehydrogenation of n-butane on MgO-supported vanadium oxide catalysts. Catal. Today 40 (1998): 215-228.

Nieto, J.M.L.; Soler, J.; Concepcion, P.; Herguido, J.; Menendez, M.; and Santamaria, J. Oxidative dehydrogenation of alkanes over V-based catalysts: Influence of redox properties on catalytic performance. J. Catal. 185 (1999): 324-332.

Ostrowski, T.; Giroir-Fendler, A.; Mirodatos, C. and Mleczko, L. Comparative study of the catalytic partial oxidation of methane to synthesis gas in fixed-bed and fluidized-bed membrane reactors. Part I: A modeling approach. Catal. Today 40 (1998a): 181-190.

Ostrowski, T.; Giroir-Fendler, A.; Mirodatos, C. and Mleczko, L. Comparative study of the catalytic partial oxidation of methane to synthesis gas in fixed-bed and fluidized-bed membrane reactors. Part II: Development of membranes and catalytic measurements. Catal. Today 40 (1998a): 191-200.

Pantazidis, A.; Dalmon, J. A. and Mirodatos, C. Oxidative dehydrogenation of propane on catalytic membrane reactors. Catal. Today 25 (1995): 403-408.

Quicker, P.; Hollein, V. and Dittmeyer, R. Catalytic dehydrogenation of hydrocarbons in palladium composite membrane reactors. Catal. Today 56 (2000): 21-34.

Ramachandra, A.M.; Lu, Y.; Ma, Y.H.; Moser, W.R. and Dixon, A.G. Oxidative coupling of methane in porous vycor membrane reactors. J. Membrane Sci. 116 (1996): 253-264.

Ramos, R.; Menendez, M. and Santamaria, J. Oxidative dehydrogenation of propane in an inert membrane reactor. Catal. Today 56 (2000): 239-245.

Robert C. Reid; John M. Prausnitz and Bruce E. Poling The properties of gases and liquids. (n.p.): McGraw-Hill Book Company, (1988).

Santamaria, J.; Coronas, J. Catalytic reactors based on porous ceramic membranes. Catal. Today 51 (1999): 377-389.

Saracco, G.; Neomagus, H.W.J.P.; Versteeg, G.F.; Van Swaaij, W.P.M. High-temperature membrane reactors: potential and problems. Chem. Eng. Sci. 54 (1999): 1997-2017.

Schramm, O. and Seidel-Morgenstern, A. Comparing porous and dense membranes for the application in membrane reactors. Chem. Eng. Sci. 54 (1999): 1447-1453.

Smith, J.M. and Van Ness, H.C., Introduction to chemical engineering thermodynamics. (n.p.): McGraw-Hill Book Company, (1987).

Soria, R. Overview on industrial membranes. Catal. Today 25 (1995): 285-290.

Tellez, C.; Menendez, M. and Santamaria, J. Oxidative dehydrogenation of butane using membrane reactors. 1997, 43, AIChE. J. 43 (1997): 777-784.

Tellez, C.; Menendez, M. and Santamaria, J. Simulation of an inert membrane reactor for the oxidative dehydrogenation of butane. Chem. Eng. Sci. 54 (1999a): 2917-2925.

Tellez, C.; Menendez, M. and Santamaria, J. Kinetic study of the oxidative dehydrogenation of butane on V/MgO catalysts. J. Catal. 183 (1999b): 210-221.

Tonkovich, A.L.Y.; Secker, R. B.; Reed, E.L.; Roberts, G.L. and Cox, J.L. Membrane reactor/separator: A design for bimolecular reactant addition. Sep. Sci. Technol. 30 (1995): 1609-1624.

Tonkovich, A.L.Y.; Zilka, J.L.; Jimenez, D.M. and Gary, L. Experimental investigations of inorganic membrane reactors : A distributed feed approach for partial oxidation reactions. Chem. Eng. Sci. 51 (1996a): 789-806.

Tonkovich, A.L.Y.; Jimenez, D.M.; Zilka, J.L. and Roberts, G.L. Inorganic membrane reactors for the oxidative coupling of methane. Chem. Eng. Sci. (1996b): 3051-3056.

Uemiya, S.; Sato, N. and Anto, N. Stream reforming of methanol in a hydrogen permeable membrane reactor. Appl. Catal. 67 (1991): 223.

Valenzuela, R.X.; Mamedov, E.A. and Cortes Corberan, V. Effect of different additives on the performance of V-Mg-O catalysts in the oxidative dehydrogenation of propane. React. Kinet. Catal. Lett. 55 (1995): 213-220.

Vrieland, G.E. and Murchison, C.B. Anaerobic oxidation of butane to butadiene over

magnesium molybdate catalysts. I. Magnesia supported catalysts. <u>Appl. Catal.</u> 134 (1996): 101.

Wang, W. and Lin, Y.S. Analysis of oxidative coupling of methane in dense oxide membrane reactors. <u>J. Membrane Sci.</u> 103 (1995): 219-233.

Xomeritakis, G. and Lin, Y.-S. CVD synthesis and gas permeation properties of thin palladium/alumina membranes. <u>AIChE. J.</u> 44 (1998): 174-183.

Xu, S.J. and Thomson, W.J. Perovskite-type oxide membranes for the oxidative coupling of methane. <u>AIChE. J.</u> 43 (1997): 2731-2740.

Xu, S.J. and Thomson, W.J. Oxygen permeation rates through ion-conducting perovskite membranes. <u>Chem. Eng. Sci.</u> 54 (1999): 3839-3850.

Yang, C.; Xu, N. and Shi, J. Experimental and modeling study on a packed-bed membrane reactor for partial oxidation of methane to formaldehyde. <u>Ind. Eng. Chem. Res.</u> 37 (1998): 2601-2610.

Zeng, Y.; Lin, Y.S. and Swartz, S.L. Perovskite-type ceramic membrane: synthesis, oxygen permeation and membrane reactor performance for oxidative coupling of methane. <u>J. Membrane Sci.</u> 150 (1998): 87-98.
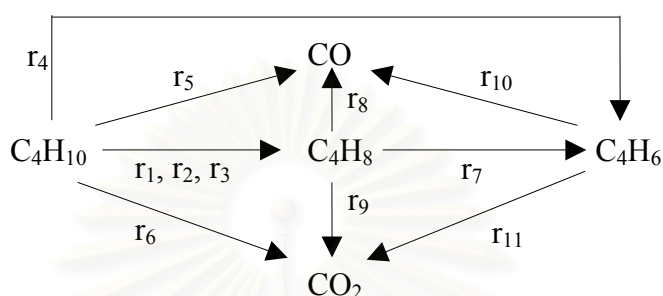
APPENDICES

APPENDIX A

RATE EXPRESSION AND HEAT OF REACTION

The rate expressions of the oxidative dehydrogenation of n-butane on V/MgO as shown in the above scheme are given in Table A-1 (Tellez *et al.,* 1999b). the reactions 1,2 and 3 refer respectively to the formation of 1-butene, cis-2-butene and trans-2-butene from n-butane.

Table A-1 Rate expression and kinetic parameters.

Reactions	Rate expression	$k_{i0} *10^3$ (mol/s kg)	E_{ai} (kJ/mol)
$C_4H_{10} + X_0 \rightarrow$ 1-C_4H_8 + H_2O + X	$r_1 = k_1 * P_{C_4H_{10}} * \theta_0$	62.33	144.9
$C_4H_{10} + X_0 \rightarrow$ Trans-2-C_4H_8 + H_2O + X	$r_2 = k_2 * P_{C_4H_{10}} * \theta_0$	32.83	142.7
$C_4H_{10} + X_0 \rightarrow$ Cis-2-C_4H_8 + H_2O + X	$r_3 = k_3 * P_{C_4H_{10}} * \theta_0$	39.67	139.1
$C_4H_{10} + 2X_0 \rightarrow C_4H_6$ + $2H_2O$ + 2X	$r_4 = k_4 * P_{C_4H_{10}} * \theta_0$	30.83	148.5
$C_4H_{10} + 9Z_0 \rightarrow$ 4CO + $5H_2O$ + 9Z	$r_5 = k_5 * P_{C_4H_{10}} * \lambda_0$	9.17	175.5
$C_4H_{10} + 13Z_0 \rightarrow 4CO_2$ + $5H_2O$ + 13Z	$r_6 = k_6 * P_{C_4H_{10}} * \lambda_0$	25.83	138.4
$C_4H_8 + X_0 \rightarrow C_4H_6$ + H_2O + X	$r_7 = k_7 * P_{C_4H_8} * \theta_0$	685.00	164.7
$C_4H_8 + 8Z_0 \rightarrow$ 4CO + $4H_2O$ + 8Z	$r_8 = k_8 * P_{C_4H_8} * \lambda_0$	32.33	146.2
$C_4H_8 + 12Z_0 \rightarrow 4CO_2$ + $4H_2O$ + 12Z	$r_9 = k_9 * P_{C_4H_8} * \lambda_0$	115.67	107.2
$C_4H_6 + 7Z_0 \rightarrow$ 4CO + $3H_2O$ + 7Z	$r_{10} = k_{10} * P_{C_4H_6} * \lambda_0$	118.17	146.6

Reactions	Rate expression	$k_{i0} *10^3$ (mol/min.g)	E_{ai} (kJ/mol)
$C_4H_6 + 11Z_0 \rightarrow 4CO_2 + 3H_2O + 11Z$	$r_{11} = k_{11}* P_{C_4H_6} *\lambda_0$	435	102.0
$O_2 + 2X \rightarrow 2X_0$	$r_{12} = k_{12}* P_{O_2} *\theta$	2995	114.5
$O_2 + 2Z \rightarrow 2Z_0$	$r_{13} = k_{13}* P_{O_2} *\lambda$	3255	5.5

where $k_i = k_{i0}e^{-E_{ai}*(1/T-1/T_0)}$, $T_0 = 773$ K and

$$\theta_0 = \frac{2k_{12}P_{O_2}}{k_{12}P_{O_2} + (k_1 + k_2 + k_3 + 2k_4)P_{C_4H_{10}} + k_7P_{C_4H_8}}$$

$$\lambda_0 = \frac{2k_{13}P_{O_2}}{k_{13}P_{O_2} + (9k_5 + 13k_6)P_{C_4H_{10}} + (8k_8 + 12k_9)P_{C_4H_8} + (7k_{10} + 11k_{11})P_{C_4H_6}}$$

Heat of reaction at constant pressure

The standard heat of reaction are the enthalpy of products subtracted with enthalpy of reactants

$$\Delta H^0 = \sum \upsilon_i \Delta H_i^0 \qquad (A-1)$$

where subscript i identifies a product or reactant and υ_i is the stoichiometric coefficient where it is positive for a product and negative for a reactant.

The enthalpies of specific species can be shown as the function of temperature by

$$dH_i^0 = C_{pi}dT \qquad (A-2)$$

and summing over all products and reactants gives

$$d\sum \upsilon_i H_i^0 = \sum \upsilon_i C_{pi}dT \qquad (A-3)$$

The term $\sum \upsilon_i H_i^0$ is the standard heat of reaction that defines in Eq. (A-1). Similarly, the capacity change of reaction as

$$\Delta C_p = \sum \upsilon_i C_{pi} \qquad (A-4)$$

As a result of these definitions, the preceding equation becomes

$$d\Delta H^0 = \Delta C_p dT \qquad \text{(A-5)}$$

This is the fundamental equation relating heat of reaction to temperature. Integration between 298 K and temperature T gives.

$$\int_{\Delta H_{298}^0}^{\Delta H_T} d\Delta H^0 = \int_{298}^{T_2} \Delta C_p dT \qquad \text{(A-6)}$$

$$\Delta H_T = \Delta H_{298}^0 + \int_{298}^{T_2} C_p dT \qquad \text{(A-7)}$$

$$\Delta C_{p,m} = \frac{\int_{T_1}^{T_2} C_p dT}{T_2 - T_1} ; \qquad T_1 = 298\ \text{K} \qquad \text{(A-8)}$$

The subscript "m" denotes a mean value specific to enthalpy calculation. Then the heat of reaction as function of temperature is shown below.

$$\Delta H_T = \Delta H_{298}^0 + \Delta C_{p,m}(T - 298) \qquad \text{(A-9)}$$

where $\Delta H_{298}^0 = H_{product,298}^0 - H_{reac\tan t,298}^0$

The heat of formation at 298 K and heat capacities of gases are shown in Table A-2 (Smith *et al.,* 1987).

Table A-2 Heat of formation and heat capacities of gases (Smith *et al.,* 1987).

Chemical species	H^o_{298} (kJ/mol)	Tmax K	A	10^3*B	10^6*C	$10^{-6}*D$	$10^{-5}*E$
n-C_4H_{10}	-125.79	1500	1.935	36.915	-11.402	-	-
1-C_4H_8	-0.54	1500	1.967	31.63	-9.873	-	-
t-C_4H_8	-10.06	1500	1.085	36.621	-17.377	0.0134	-
c-C_4H_8	-5.7	1500	-0.958	40.726	-20.447	0.0142	-
C_4H_6	109.24	1500	2.734	26.786	-8.882	-	-
O_2	0	2000	3.639	0.506	-	-	-0.227
CO	-110.53	2500	3.376	0.557	-	-	-0.031
CO_2	-393.51	2000	5.457	1.045	-	-	-1.157
H_2O	-241.82	2000	3.47	1.45	-	-	0.121
N_2	0	2000	3.28	0.593	-	-	0.04

where $C_{pi}/R_{gas} = A + BT + CT^2 + DT^3 + ET^{-2}$ and R_{gas} = 8.314 J mol^{-1} K^{-1}

APPENDIX B
OVERALL HEAT TRANSFER COEFFICIENT

The overall heat transfer coefficients include heat convection and heat conduction. U_{SS} and U_M are the overall heat transfer coefficient through stainless steel and alumina membrane respectively.

For Fixed-bed Reactor:
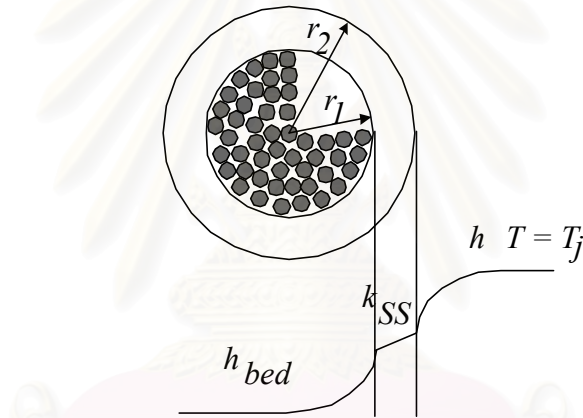
Figure B-1 Schematic diagram of heat transfer in the fixed-bed Reactor.

$$\frac{1}{U_{SS}A_{P1}} = \frac{1}{h_{bed}A_{P1}} + \frac{\ln(r_2/r_1)}{2\pi k_{SS}L} \tag{B-1}$$

$$A_{P1} = 2\pi r_1 L$$

$$\Pr = \frac{C_p\mu}{\lambda_g}; \qquad \mathrm{Re} = \frac{4\dot{m}}{\pi D\mu}$$

$$D = \frac{4A_C}{\Gamma}$$

where C_p, λ_g and μ are the heat capacity, thermal conductivity, and viscosity of mixture gas, respectively, whose values can be calculated as described in Appendix C.

In addition, $\dot{m}$ is the total mass flow rate, A_C is the flow cross-sectional area and Γ is the wetted perimeter.

Nu_{bed}, h_{bed} (Koukou et al., 1995)

$$\text{Re}_{d_P} = \frac{4\dot{m}d_P}{\pi D^2 \mu_m};$$

d_p is particle diameter

$$Nu_{bed} = \frac{h_{bed}d_P}{\lambda_g} = 5\,\text{Re}_{d_P}^{0.365} \qquad\qquad (B\text{-}2)$$

The data of thermal conductivity of stainless steel (k_{SS}) and alumina membrane (k_M) can be giving by MILLS, 1995 in W/mK unit as shown in Table B-1 and Figure B-2.

Table B-1 Thermal conductivity.

Temperature (K)	Stainless Steel AISI 304 (W/m K)	Al$_2$O$_3$ (W/m K)
300	15	36
400	17	27
500	18	
600	20	16
800	23	
1000	25	7.6
1500		5.4
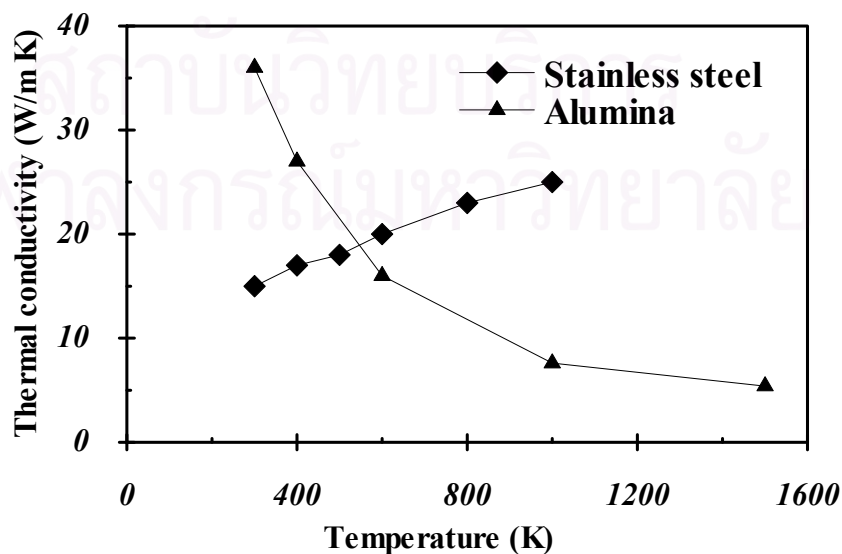
Figure B-2 Thermal conductivity of stainless steel and alumina.

$$k_{SS} = -5 \times 10^{-6}\left(T^2\right) + 0.0215(T) + 9.0303 \tag{B-3}$$

$$k_M = 111058(T)^{-1.3867} \tag{B-4}$$

<u>For Inert Membrane Reactor</u>:
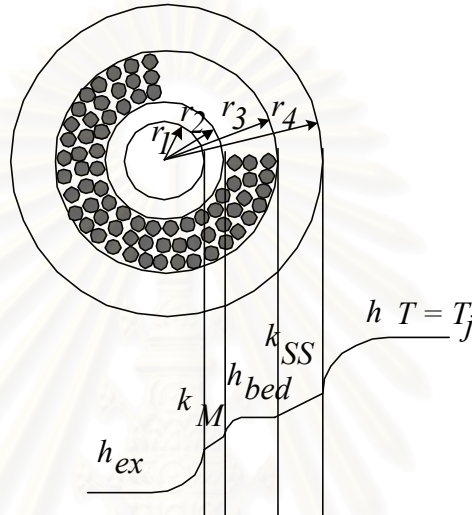
Figure B-3 Schematic diagram of heat transfer in Inert Membrane Reactor.

$$\frac{1}{U_M A} = \frac{1}{h_{bed} A_{P1}} + \frac{\ln(r_2/r_1)}{2\pi k_M L} + \frac{1}{A_{P2} h_{ex}} \tag{B-5}$$

where $A_{P1} = 2\pi r_1 L$; $A_{P2} = 2\pi r_2 L$

$$\frac{1}{U_{SS} A_{P3}} = \frac{1}{h_{bed} A_{P3}} + \frac{\ln(r_4/r_3)}{2\pi k_{SS} L} \tag{B-6}$$

$$A_{P3} = 2\pi r_3 L$$

The h_{bed}, Re, Pr and D are similarly denoted as above. In addition k_M is used in Equation B-4.

<u>Nu_{ex}, h_{ex} (Frank P. I. and David P. De Witt (1990))</u>

For $0.5 < Pr < 2000$ and $2300 < Re < 5 \times 10^6$

$$Nu_{ex} = \frac{h_{ex} D}{\lambda_g} = \frac{(f/8)(Re - 1000)Pr}{1 + 12.7(f/8)^{1/2}\left(Pr^{2/3} - 1\right)} \tag{B-7}$$

$$f = (0.79 \ln \text{Re} - 1.64)^{-2}$$

For 0.5 < Pr < 2000 and Re < 2300

$$Nu_{ex} = \frac{h_{ex}D}{\lambda_g} = 3.66 + \frac{0.0668(D/L)\text{Re}\,\text{Pr}}{1 + 0.04\left[(D/L)\text{Re}\,\text{Pr}\right]^{2/3}} \qquad \text{(B-8)}$$

APPENDIX C
PHYSICAL PROPERTIES

The Appendix summarizes necessary information for the simulation. All properties of the viscosity, diffusion coefficient and thermal conductivity for low to moderate pressure are obtained from Robert C. Reid, John M. Prausnitz and Bruce E. Poling (1988).

1. Viscosity of gases

<u>Pure gas component</u>

The viscosity of gases at low pressure is described below.

$$\mu_i = 40.785 \frac{F_c(MT)^{1/2}}{V_c^{2/3}\Omega_v} \qquad \text{C-1}$$

where μ = viscosity of pure gas i, cP

M = molecular weight, g/mole

T = temperature, K

V_c = critical volume, m³/mole

ω = acentric factor

η = dipole moment, debye

$$\Omega_v = \left[A\left(T_v^*\right)^{-B}\right] + C\left[\exp\left(-DT_v^*\right)\right] + E\left[\exp\left(-FT_v^*\right)\right] \qquad \text{C-2}$$

where Ω_v = viscosity collision

$A = 1.16145$, $B = 0.14874$, $C = 0.52487$, $D = 0.77320$, $E = 2.16178$ and $F = 2.43787$

$$T_v^* = 1.2593T_r \qquad \text{C-3}$$

$$F_c = 1 - 0.2756\omega + 0.059035\eta_r^4 + \kappa \qquad \text{C-4}$$

The term η_r is a dimensionless dipole moment.

$$\eta_r = 131.3 \frac{\eta}{(V_cT_c)^{1/2}} \qquad \text{C-5}$$

All species in this system the value of a special correction for highly polar substances (κ) in Equation C-4 was zero except water, κ was 0.076.

Gas mixture

The viscosity of gas mixture at low pressure is shown in below.

$$\mu_m = \sum_{i=1}^{n} K_i \left(1 + 2\sum_{j=1}^{i-1} H_{ij}K_j + \sum_{\substack{j=1 \\ \neq i}}^{n} \sum_{\substack{k=1 \\ \neq i}}^{n} H_{ij}H_{ik}K_jK_k \right) \qquad \text{C-6}$$

where μ_m is the viscosity of gas mixture, M_i is the molecular weight of i, and y_i is the mole fraction of i in the mixture.

$$K_i = \frac{y_i \mu_i}{y_i + \mu_i \sum_{\substack{k=1 \\ \neq i}}^{n} y_k H_{ik}[3 + (2M_k/M_i)]} \qquad \text{C-7}$$

The other component properties used are:

$$U_i = \frac{[1 + 0.36T_{ri}(T_{ri} - 1)]^{1/6} F_{Ri}}{(T_{ri})^{1/2}} \qquad \text{C-8}$$

$$E_i = \frac{M_i^{1/4}}{(\mu_i U_i)^{1/2}} \qquad \text{C-9}$$

where $T_{ri} = T/T_{ci}$ and F_{Ri} is a polar correction.

$$F_{Ri} = \frac{T_{ri}^{3.5} + (10\eta_{ri})^7}{T_{ri}^{3.5}[1 + (10\eta_{ri})^7]} \qquad \text{C-10}$$

Here η_{ri} is the reduced dipole moment of i.

$$\eta_{ri} = 52.46\frac{\eta^2 P_c}{T_c^2} \qquad \text{C-11}$$

For the term $H_{ij} = H_{ji}$,

$$H_{ij} = \left[\frac{M_i M_j}{32(M_i + M_j)^3} \right]^{1/2} (E_i + E_j)^2 \times \frac{[1 + 0.36T_{rij}(T_{rij} - 1)]^{1/6} F_{Rij}}{(T_{rij})^{1/2}} \qquad \text{C-12}$$

with $\quad T_{rij} = \dfrac{T}{(T_{ci}T_{cj})^{1/2}} \qquad \text{C-13}$

$$\eta_{rij} = (\eta_{ri}\eta_{rj})^{1/2} \qquad \text{C-14}$$

F_{Rij} was found from Equation C-10 with T_{ri} replaced by T_{rij} and η_{ri} by η_{rij}.

2. Diffusion coefficients

Binary gas

The correlation describing diffusion coefficient of binary gas at low to moderate pressure has been expressed below.

$$D_{ij} = \frac{0.00266T^{3/2}}{PM_{ij}^{1/2}\sigma_{ij}^2\Omega_D} \qquad \text{C-15}$$

where D_{ij} = diffusion coefficient of binary gas, m²/s

M_i, M_j = molecular weights of i and j

V_b = liquid molar volume at the normal boiling point, m³/mol

T_b = normal boiling point (101.3 kPa), K

σ_{ij} = characteristic length, A

η = dipole moment, debyes

P = pressure, kPa

$$M_{ij} = 2\left[\left(1/M_i\right) + \left(1/M_j\right)\right]^{-1}$$

$$\Omega_D = \frac{A}{\left(T_D^*\right)^B} + \frac{C}{\exp\left(DT_D^*\right)} + \frac{E}{\exp\left(FT_D^*\right)} + \frac{G}{\exp\left(HT_D^*\right)} + \frac{0.19\delta_{ij}^2}{T_D^*} \qquad \text{C-16}$$

where $A = 1.06036$, $B = 0.15610$, $C = 0.19300$, $D = 0.47635$, $E = 1.03587$, $F = 1.52996$, $G = 1.76474$ and $H = 3.89411$

$$T_D^* = \frac{kT}{\varepsilon_{ij}} \qquad \text{C-17}$$

$$\delta = \frac{1.94 * 10^3 \eta^2}{V_b T_b} \qquad \text{C-18}$$

$$V_b = 0.285V_c^{1.048}$$

$$\frac{\varepsilon}{k} = 1.18\left(1 + 1.3\delta^2\right)T_b \qquad \text{C-19}$$

$$\sigma = \left(\frac{1.585V_b}{1 + 1.3\delta^2}\right)^{1/3} \qquad \text{C-20}$$

$$\delta_{ij} = \left(\delta_i \delta_j\right)^{\frac{1}{2}} \hspace{6cm} \text{C-21}$$

$$\frac{\varepsilon_{ij}}{k} = \left(\frac{\varepsilon_i}{k}\frac{\varepsilon_j}{k}\right)^{\frac{1}{2}} \hspace{5cm} \text{C-22}$$

$$\sigma_{ij} = \left(\sigma_i \sigma_j\right)^{\frac{1}{2}} \hspace{6cm} \text{C-23}$$

Gas mixture and effective radial diffusion coefficient

$$\frac{1-y_i}{D_{i,m}} = \sum_{j=2}^{n} \frac{y_i}{D_{ij}} \hspace{5cm} \text{C-24}$$

The effective radial diffusion coefficient can be described in the following correlation (Itoh *et al.,* 1994).

$$1/\text{Pe}_r = 0.4/(\text{Re}_p\text{Sc})0.8+0.009/\{1+10/(\text{Re}_p\text{Sc})\} \hspace{1cm} \text{C-25}$$

for $0.4 < \text{Re}_p < 500$, $0.77 < \text{Sc} < 1.2$

where

$D_{i,m}$ = diffusion coefficient of gas mixture, m^2/s

D_{er} = effective radial diffusion coefficient, m^2/s

y_i, y_j = mole fraction of components i and j

Pe_r = Peclet number, ud_p/D_{er}

Sc = Schmidt number, $\mu/\left(\rho D_{i,m}\right)$

$$\text{Re}_p = \frac{\rho u d_p}{\mu_m}$$

u = velocity of gas, m/s

d_p = particle diameter, m

3. Thermal conductivity

Pure component

The correlation for thermal conductivity of pure gas component and solid catalyst are given by Carl L. Yaws (1999).

$$\lambda_i = A_i + B_i T + C_i T^2, \text{ W/(m K)} \hspace{4cm} \text{C-26}$$

Table C-1 Thermal conductivity of pure gas component and solid catalyst.

Species	A	B	C
n-Butane	-0.00182	1.9396E-5	1.3818E-7
1-Butene	-0.00293	3.0205E-5	1.0192E-7
c-Butene	-0.02545	1.2682E-4	2.2968E-9
t-Butene	-0.02331	1.2197E-4	4.7243E-9
1,3-Butadiene	-0.00085	7.1537E-6	1.6202E-7
Oxygen	0.00121	8.6157E-5	-1.3346E-8
Carbon monoxide	0.00158	8.2511E-5	-1.9081E-8
Carbon dioxide	-0.012	1.0208E-4	-2.2403E-8
Water	0.00053	4.7093E-5	4.9551E-8
Nitrogen	0.00309	4.75E-1	-1.1014E-8

Gas mixture and effective radial thermal conductivity

$$\lambda_m = \sum_{i=1}^{n} \frac{y_i \lambda_i}{\sum_{j=1}^{n} y_j A_{ij}} \qquad \text{C-27}$$

λ_m = thermal conductivity of the gas mixture, W/(m K)

λ_{sc} = thermal conductivity of solid catalyst, assume equal to MgO, W/(m K)

λ_{er} = effective radial thermal conductivity, W/(m K)

y_i, y_j = mole fraction of components i and j

$$A_{ij} = \frac{\left[1 + \left(\varphi_{tri}/\varphi_{trj}\right)^{1/2}\left(M_i/M_j\right)^{1/4}\right]^2}{\left[8\left(1 + M_i/M_j\right)\right]^{1/2}} \qquad \text{C-28}$$

$A_{ii} = 1$

where φ_{tr} is monatomic value of the thermal conductivity.

$$\frac{\varphi_{tri}}{\varphi_{trj}} = \frac{\Lambda_j \left[\exp(0.0464T_{ri}) - \exp(-0.2412T_{ri})\right]}{\Lambda_i \left[\exp(0.0464T_{rj}) - \exp(-0.2412T_{rj})\right]} \qquad \text{C-29}$$

and Λ is defined by the following equation.

$$\Lambda = 210 \left(\frac{T_c M^3}{P_c^4} \right)^{1/6} \qquad \text{C-30}$$

The effective radial thermal conductivity is considered to consist of two contributions, the first static and the second dynamic (i.e., dependent on the flow conditions), so that (Froment, G. F. and Bischoff, K. B. (1990))

$$\lambda_{er} = \lambda_{er}^0 + \lambda_{er}^t \qquad \text{C-31}$$

$$\frac{\lambda_{er}^0}{\lambda_m} = \left(1 - \sqrt{1-\varepsilon}\right)\left(1 + \varepsilon \frac{\alpha_{rs} d_p}{\lambda_m}\right) + \frac{2\sqrt{1-\varepsilon}}{1 + \left(\frac{\alpha_{rs} d_p}{\lambda_m} - B\right)\frac{\lambda_m}{\lambda_{sc}}} \theta \qquad \text{C-32}$$

$$\alpha_{rs} = 0.227 \frac{\varepsilon_r}{2-\varepsilon_r} \left(\frac{T}{100}\right)^3 \qquad \text{C-33}$$

where ε_r is the emissivity of the solid and α_{rs} is radiation coefficient for the solid.

$$\text{C-34}$$

$$\theta = \frac{\left[1 + \left(\frac{\alpha_{rs} d_p}{\lambda_m} - 1\right)\frac{\lambda_m}{\lambda_{sc}}\right] B}{\left[1 + \left(\frac{\alpha_{rs} d_p}{\lambda_m} - B\right)\frac{\lambda_m}{\lambda_{sc}}\right]^2} \ln\left(\frac{1 + \frac{\alpha_{rs} d_p}{\lambda_{sc}}}{B \frac{\lambda_m}{\lambda_{sc}}}\right) - \frac{B-1}{1 + \left(\frac{\alpha_{rs} d_p}{\lambda_m} - B\right)\frac{\lambda_m}{\lambda_{sc}}} + \frac{B+1}{2B}\left(\frac{\alpha_{rs} d_p}{\lambda_m} - B\right)$$

$$B = b\left[\frac{1-\varepsilon}{\varepsilon}\right]^{10/9} \qquad \text{C-35}$$

$b = 1.25$ for spheres

$$\lambda_{er}^t = \varepsilon \rho C_p D_{er} \qquad \text{C-36}$$

Table C-2 The property data of gases by Robert C. Reid, John M. Prausnitz and Bruce E. Poling (1988).

No.	Formula	Name	M g/mole	T_b (K)	T_c (K)	$P_c \times 10^{-2}$ KPa	$V_c \times 10^6$ m³/mol	Acentric factor	Dipm×10³ debye
1	$n\text{-}C_4H_{10}$	n-Butane	58.124	272.7	425.2	38.0	255	0.199	0.0
2	$1\text{-}C_4H_8$	1-Butene	56.108	266.9	419.6	40.2	240	0.191	0.3
3	$c\text{-}C_4H_8$	2-Butene,cis	56.108	276.9	435.6	42.0	234	0.202	0.3
4	$t\text{-}C_4H_8$	2-Butene,trans	56.108	274.0	428.6	39.9	238	0.205	0.0
5	C_4H_6	1,3-Butadiene	54.092	268.7	425.0	43.3	221	0.195	0.0
6	O_2	Oxygen	31.999	90.2	154.6	50.4	73.4	0.025	0.0
7	CO	Carbon monoxide	28.010	81.7	132.9	35.0	93.2	0.066	0.1
8	CO_2	Carbon dioxide	44.010	194.6	304.1	73.8	93.9	0.239	0.0
9	H_2O	Water	18.015	373.2	647.3	221.2	57.1	0.344	1.8
10	N_2	Nitrogen	28.013	77.4	126.2	33.9	89.8	0.039	0.0

APPENDIX D
MATHEMATICAL MODEL

1. Fixed-bed reactor (FBR)
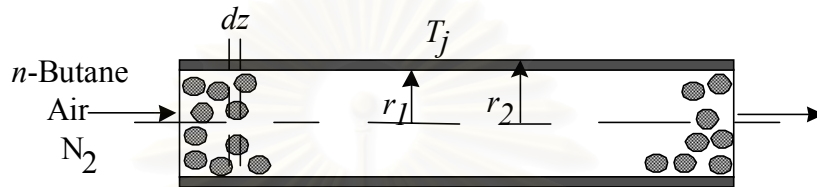
Figure D-1 Schematic diagram of Fixed-bed Reactor.

<u>1.1 Plug flow model</u>

<u>Mass balances of species i</u>

The mole balance of oxidative dehydrogenation reaction is made in a small element of length dz with a rate of formation of specie i (r_i) that shows in Figure D-1.

$$F_i|_z - F_i|_{z+dz} + \rho_B r_i (\pi r_1^2 dz) = 0 \tag{D-1}$$

The subscripts, z and $z+dz$, represent the position of interest, i refers to each species and r_i is rate of formation. The catalyst bed density is ρ_B. The equation (D-1) can be written in the differential forms as shown below.

$$\frac{dF_i}{dz} = \pi r_1^2 \rho_B r_i \tag{D-2}$$

<u>Energy balance</u>

$$\sum_{i=1}^{n} (F_i C_{pi})(T - 298)_z - \sum_{i=1}^{n} (F_i C_{pi})(T - 298)_{z+\Delta z} + U_{SS}(T_j - T)2\pi r_1 dz$$

$$+ \rho_B \pi r_1^2 dz \sum_{i=1}^{n} (R_i(-\Delta H_{ri})) = 0 \tag{D-3}$$

where R_i and ($-\Delta H_{ri}$) are the rate of reaction and the heat of reaction of the reaction i, respectively as show in Appendix A. The temperature of external wall of reactor is equal to the ambient temperature, T_j. The differential form is

$$\sum_{i=1}^{n} F_i C_{pi} \frac{dT}{dz} = \rho_B \pi r_1^2 \sum_{i=1}^{n} R_i \left(-\Delta H_{ri}\right) + U_{SS} 2\pi r_1 \left(T_j - T\right) \tag{D-4}$$

U_{SS} is overall heat transfer coefficient through stainless steel shown in Appendix B.

1.2 Radial diffusion model
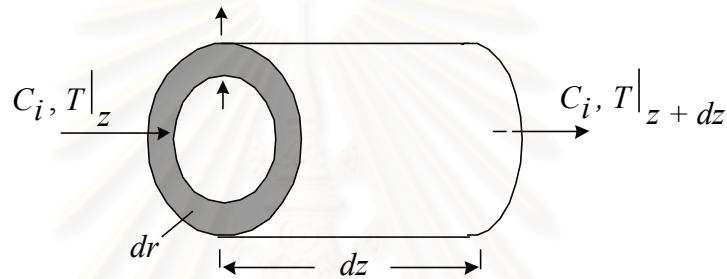
Figure D-2 Schematic diagram of control volume for radial diffusion model.

Mass balances of species i

The mole balance of the oxidative dehydrogenation reaction for the product i in the reactor segment between z and $z + \Delta z$, r and $r + \Delta r$, θ and $\theta + \Delta\theta$ with a rate of formation (r_i) as shown in Figure D-2 is:

Radial output – input $\quad = -D_{er}(2\pi dz)d\left(r\frac{\partial C_i}{\partial r}\right)$

Axial output – input $\quad = -D_e(2\pi r dr)d\left(\frac{\partial C_i}{\partial z}\right) + (2\pi r dr)\frac{dF_i}{A_C}$

Sink $\quad = \rho_B(dV_r)r_i \quad = \rho_B(2\pi r dr dz)r_i$

Accumulation $\quad = (dV_r)\frac{\partial C_i}{\partial t} \quad = (2\pi r dr dz)\frac{\partial C_i}{\partial t}$

Putting these elements together and dividing by $2\pi r dr dz$ gives

$$-\frac{D_{er}}{r}\frac{\partial}{\partial r}\left(r\frac{\partial C_i}{\partial r}\right) - D_e\left(\frac{\partial^2 C_i}{\partial z^2}\right) + \frac{1}{A_C}\frac{\partial F_i}{\partial z} - \rho_B r_i + \frac{\partial C_i}{\partial t} = 0 \tag{D-5}$$

and including the assumptions in Chapter IV the following form is obtained.

$$\frac{1}{A_C}\frac{\partial F_i}{\partial z} - D_{er}\left(\frac{1}{r}\frac{\partial C_i}{\partial r} + \frac{\partial^2 C_i}{\partial r^2}\right) - \rho_B r_i = 0 \tag{D-6}$$

For fixed-bed reactor $A_C = \pi r_1^2$.

$$C_i = \frac{p_i}{R_{gas}T} = \frac{F_i}{F_T}\frac{P_T}{R_{gas}T} \tag{D-7}$$

where P_T and R_{gas} are total pressure and gas constant respectively.

Substitute equation (D-7) into (D-6) and rearrange to the new form.

$$\frac{\partial F_i}{\partial z} = D_{er}\pi r_1^2 \frac{P_T}{R_{gas}}\left[\frac{1}{r}\frac{\partial}{\partial r}\left(\frac{F_i}{F_T T}\right) + \frac{\partial^2}{\partial r^2}\left(\frac{F_i}{F_T T}\right)\right] + \pi r_1^2 \rho_B r_i \tag{D-8}$$

B.C. $z = 0$; $\qquad C_i = C_{i,0}$; $\qquad F_i = F_{i,0}$ $\qquad$ for all r

$\qquad r = 0$; $\qquad \dfrac{\partial C_i}{\partial r} = 0$; $\dfrac{\partial}{\partial r}\left(\dfrac{F_i}{F_T T}\right) = 0$ $\qquad$ for all z

$\qquad r = r_1$; $\qquad \dfrac{\partial C_i}{\partial r} = 0$; $\dfrac{\partial}{\partial r}\left(\dfrac{F_i}{F_T T}\right) = 0$ $\qquad$ for all z

<u>Energy balance</u>

The elements of the energy balance consist of the following four terms.

Radial output – input $\quad = -\lambda_{er}(2\pi dz)d\left(r\dfrac{\partial T}{\partial r}\right)$

Axial output – input $\quad = -\lambda_e(2\pi rdr)d\left(\dfrac{\partial T}{\partial z}\right) + \sum\limits_{i=1}^{n}\left(\dfrac{F_i C_{Pi}}{A_C}\right)(2\pi rdr)dT$

$\qquad\qquad$ Sink $\quad = \sum\limits_{i=1}^{n}\left((-\Delta H_{ri})R_i\right)\rho_B dV_r$

$\qquad\qquad\qquad = \sum\limits_{i=1}^{n}\left((-\Delta H_{ri})R_i\right)\rho_B(2\pi rdrdz)$

$\qquad$ Accumulation $\quad = \rho C_P dV_r \dfrac{\partial T}{\partial t} = \rho C_P(2\pi rdrdz)\dfrac{\partial T}{\partial t}$

Putting these elements together and dividing by $2\pi rdrdz$ results in

$$-\frac{\lambda_{er}}{r}\frac{\partial}{\partial r}\left(r\frac{\partial T}{\partial r}\right) - \lambda_e\left(\frac{\partial^2 T}{\partial z^2}\right) + \sum\limits_{i=1}^{n}\left(\frac{F_i C_{Pi}}{A_C}\right)\frac{\partial T}{\partial z} - \rho_B\sum\limits_{i=1}^{n}\left((-\Delta H_{ri})R_i\right) + \rho_B C_p\frac{\partial T}{\partial t} = 0$$

$$\tag{D-9}$$

and from the assumptions the following equations are obtained.

$$\sum_{i=1}^{n}\left(\frac{F_i C_{Pi}}{A_C}\right)\frac{\partial T}{\partial z} = \frac{\lambda_{er}}{r}\frac{\partial}{\partial r}\left(r\frac{\partial T}{\partial r}\right) + \rho_B \sum_{i=1}^{n}\left((-\Delta H_{ri})R_i\right)$$

$$\frac{\partial T}{\partial z} = \frac{A_C}{\sum_{i=1}^{n}\left(F_i C_{Pi}\right)}\lambda_{er}\left[\frac{1}{r}\frac{\partial T}{\partial r}+\frac{\partial^2 T}{\partial r^2}\right] + \rho_B \sum_{i=1}^{n}\left((-\Delta H_{ri})R_i\right)\frac{A_C}{\sum_{i=1}^{n}\left(F_i C_{Pi}\right)} \quad \text{(D-10)}$$

B.C. $z = 0;$ $T = T_0$ for all r

   $r = 0$; $\dfrac{\partial T}{\partial r} = 0$ for all z

   $r = r_1;$ $-\lambda_{er}\dfrac{\partial T}{\partial r} = U_{SS}\left(T_{r=r1} - T_j\right)$ for all z

2. Inert membrane reactor (IMR)
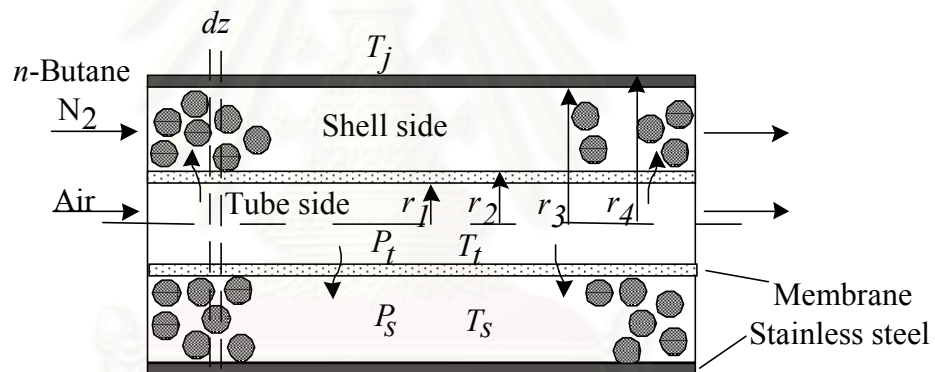
Figure D-3 Schematic diagram of Inert Membrane Reactor.

2.1 Plug flow model

In this section the energy and mass balance are similar to these of the fixed-bed reactor model but the permeation term is included. The mass and energy balances made in small dz as shown in Figure D-3 are

Mass balances of species i
Shell side:

$$F_{i,z}^{s} - F_{i,z+\Delta z}^{s} + \rho_B r_i \pi\left(r_3^2 - r_2^2\right)dz + \left(\frac{F_i}{L}\right)'dz = 0 \qquad \text{(D-11)}$$

$$\frac{dF_i^s}{dz} = \frac{\rho_B \pi (r_3^2 - r_2^2)}{4} r_i + \left(\frac{F_i}{L}\right)' \tag{D-12}$$

$$\qquad \qquad \text{rate of reaction} \quad \text{permeation}$$

Tube side:

$$F_{i,z}^t - F_{i,z+\Delta z}^t - \left(\frac{F_i}{L}\right)' dz = 0 \tag{D-13}$$

$$\frac{dF_i^t}{dz} = -\left(\frac{F_i}{L}\right)' \tag{D-14}$$

Energy balance

Shell side:

$$\sum_{i=1}^{n}\left(F_i^s C_{pi}\right)\left(T_s - 298\right)_z - \sum_{i=1}^{n}\left(F_i^s C_{pi}\right)\left(T_s - 298\right)_{z+\Delta z} + U_{SS}\left(T_j - T_s\right)2\pi r_3 dz$$

$$+ \sum_{i=1}^{n}\left(H_i\left(\frac{F_i}{L}\right)'\right)dz - U_M\left(T_s - T_t\right)2\pi r_1 dz$$

$$+ \rho_B \pi\left(r_3^2 - r_2^2\right)dz \sum_{i=1}^{n}\left(R_i\left(-\Delta H_{ri}\right)\right) = 0 \tag{D-15}$$

$$\sum_{i=1}^{n}\left(F_i^s C_{pi}\right)\frac{dT_s}{dz} = U_{SS}2\pi r_3(T_j - T_s) - U_M 2\pi r_1(T_s - T_t) + \sum_{i=1}^{n}\left(H_i\left(\frac{F_i}{L}\right)'\right)$$

$$+ \rho_B \pi\left(r_3^2 - r_2^2\right)\sum_{i=1}^{n}\left(R_i\left(-\Delta H_{ri}\right)\right) \tag{D-16}$$

Tube side:

$$\sum_{i=1}^{n}\left(F_i^t C_{pi}\right)\left(T_t - 298\right)_z - \sum_{i=1}^{n}\left(F_i^t C_{pi}\right)\left(T_t - 298\right)_{z+\Delta z} + U_M\left(T_s - T_t\right)2\pi r_1 dz$$

$$+ \sum_{i=1}^{n}\left(H_i\left(\frac{F_i}{L}\right)'\right)dz = 0 \tag{D-17}$$

$$\sum_{i=1}^{n}\left(F_i^t C_{pi}\right)\frac{dT_t}{dz} = U_M 2\pi r_1(T_s - T_t) + \sum_{i=1}^{n}\left(H_i\left(\frac{F_i}{L}\right)'\right) \tag{D-18}$$

where R_i, ($-\Delta H_{ri}$) and U_M are rate of reaction i, heat of reaction of reaction *i* and over all heat transfer coefficient through the alumina membrane, respectively as shown in Appendix A and B. The temperature of external wall of reactor is equal to the ambient temperature, T_j.

2.2 Radial diffusion model

The mass balance is the same as the fixed-bed reactor but the cross sectional area (A_C) is different. For the shell side A_{C_s} is $\pi\left(r_3^2 - r_2^2\right)$ while A_{C_t} is πr_1^2 for the tube side. In the tube side of the membrane reactor, where air was fed, the plug flow condition is assumed. Hence, the equation of mass and energy balance were the same as the plug flow model. The control volume diagram for the shell side is given in Figure D-2.

Mass balances of species *i*

Shell side:

$$\frac{1}{A_{C_s}}\frac{\partial F_i^s}{\partial z} = D_{er}^s\left[\frac{1}{r}\frac{\partial C_i^s}{\partial r} + \frac{\partial^2 C_i^s}{\partial r^2}\right] + \rho_B r_i$$

$$\frac{\partial F_i^s}{\partial z} = D_{er}^s\pi\left(r_3^2 - r_2^2\right)\frac{P_s}{R_{gas}}\left[\frac{1}{r}\frac{\partial}{\partial r}\left(\frac{F_i^s}{F_i^s T_s}\right) + \frac{\partial^2}{\partial r^2}\left(\frac{F_i^s}{F_T^s T_s}\right)\right] + \pi\left(r_3^2 - r_2^2\right)\rho_B r_i \quad \text{(D-19)}$$

B.C. $z = 0$; $\qquad C_i^s = C_{i,0}^s$; $\quad F_i^s = F_{i,0}^s \qquad$ for all r

$\qquad r = r_2$; $\qquad \dfrac{\partial C_i^s}{\partial r} = \dfrac{P_s}{R_{gas}}\dfrac{\partial}{\partial r}\left(\dfrac{F_i^s}{F_i^s T_s}\right) = -\dfrac{1}{D_{er}^s 2\pi r_2}\left(\dfrac{F_i}{L}\right)' \quad$ for all z

$\qquad r = r_3$; $\qquad \dfrac{\partial C_i^s}{\partial r} = 0$; $\quad \dfrac{\partial}{\partial r}\left(\dfrac{F_i^s}{F_i^s T_s}\right) = 0 \quad$ for all z

P_t and P_s are total pressure at the tube and shell sides, respectively.

Energy balance

Shell side:

$$\frac{\partial T_s}{\partial z} = \frac{\pi\left(r_3^2 - r_2^2\right)}{\sum_{i=1}^{n}\left(F_i^s C_{Pi}\right)} \lambda_{er}^s \left[\frac{1}{r}\frac{\partial T_s}{\partial r} + \frac{\partial^2 T_s}{\partial r^2}\right] + \rho_B \sum_{i=1}^{n}\left((-\Delta H_{ri})R_i\right)\frac{\pi\left(r_3^2 - r_2^2\right)}{\sum_{i=1}^{n}\left(F_i^s C_{Pi}\right)} \qquad \text{(D-20)}$$

B.C. $\quad z = 0 \qquad\qquad T_s = T_{s,0} \qquad\qquad \text{for all } r$

$\quad r = r_2 ;$

$$-\lambda_{er}^s \frac{\partial T_s}{\partial r} = U_M\left(T_{t\,r=r_1} - T_{s\,r=r_2}\right) + \sum \frac{1}{2\pi r_2}\left(\frac{F_i}{L}\right)' H_i \qquad \text{for all } z$$

$\quad r = r_3 ; \qquad\qquad -\lambda_{er}^s \frac{\partial T_s}{\partial r} = U_{SS}\left(T_{s\,r=r_3} - T_j\right) \quad \text{for all } z$

3. Dimensionless form

The sets of mass and heat balance both the fixed-bed reactor and the inert membrane reactor were converted to dimensionless forms by introducing the following equations.

$$\overline{F_i} = \frac{F_i}{F_{T,0}} \qquad \overline{F_T} = \frac{F_T}{F_{T,0}} \qquad \overline{F_i^t} = \frac{F_i^t}{F_{T,0}^t} \qquad \overline{F_i^s} = \frac{F_i^s}{F_{T,0}^s} \qquad \overline{F_T^t} = \frac{F_T^t}{F_{T,0}^t}$$

$$\overline{F_T^s} = \frac{F_T^s}{F_{T,0}^s} \qquad \overline{T} = \frac{T}{T_0} \qquad \overline{T_t} = \frac{T_t}{T_{t,0}} \qquad \overline{T_s} = \frac{T_s}{T_{s,0}} \qquad R = \frac{r}{r_1}$$

$$\gamma_1 = \frac{T_{t,0}}{T_{s,0}} \qquad \gamma_2 = \frac{T_{s,0}}{T_{t,0}} \qquad \overline{T_j} = \frac{T_j}{T_0} \text{ for FBR or } \overline{T_j} = \frac{T_j}{T_{s,0}} \text{ for IMR}$$

$$R_s = \frac{r}{\left(r_3 - r_2\right)} \qquad R_2 = \frac{r_2}{\left(r_3 - r_2\right)}$$

$$\alpha_{FBR} = \frac{L\pi r_1^2 D_{er} P_T}{F_{T,0} T_0 R_{gas} r_1^2} \qquad \alpha_{IMR,s} = \frac{L\pi D_{er}^s P_s}{F_{T,0}^s T_{s,0} R_{gas}}$$

$$\beta_{FBR} = \frac{L\pi r_1^2 \lambda_{er}}{r_1^2 \sum_{i=1}^{n}\left(F_i C_{pi}\right)} \qquad \beta_{IMR,s} = \frac{L\pi \lambda_{er}^s}{\sum_{i=1}^{n}\left(F_i^s C_{pi}\right)}$$

3.1 Fixed-bed reactor

$$A_C = \pi r_1^2 \qquad A_P = 2\pi r_1 L$$

Plug flow model

$$\frac{d\overline{F_i}}{d\overline{Z}} = \frac{\rho_B A_C L}{F_{T,0}} r_i \tag{D-21}$$

$$\sum\left(\overline{F_i} C_{pi}\right)\frac{d\overline{T}}{d\overline{Z}} = \frac{U_{SS} A_P}{F_{T,0}}\left(\overline{T_j} - \overline{T}\right) + \frac{A_C L \rho_B}{F_{T,0} T_0}\sum\left(R_i\left(-\Delta H_{ri}\right)\right) \tag{D-22}$$

Radial diffusion model

$$\frac{\partial \overline{F_i}}{\partial \overline{Z}} = \alpha_{FBR}\left[\frac{1}{R}\frac{\partial}{\partial R}\left(\frac{\overline{F_i}}{\overline{F_T T}}\right) + \frac{\partial^2}{\partial R^2}\left(\frac{\overline{F_i}}{\overline{F_T T}}\right)\right] + \frac{A_C L \rho_B}{F_{T,0}} r_i \tag{D-23}$$

B.C. $\overline{Z} = 0$; $\qquad \overline{F_i} = \overline{F_{i,0}}$ $\qquad (0 < R < 1)$

$\qquad R = 0$; $\qquad \dfrac{\partial}{\partial R}\left(\dfrac{\overline{F_i}}{\overline{F_T T}}\right) = 0$ $\qquad 0 < \overline{Z} < 1$

$\qquad R = 1$; $\qquad \dfrac{\partial}{\partial R}\left(\dfrac{\overline{F_i}}{\overline{F_T T}}\right) = 0$ $\qquad 0 < \overline{Z} < 1$

$$\frac{\partial \overline{T}}{\partial \overline{Z}} = \beta_{FBR}\left[\frac{1}{R}\frac{\partial \overline{T}}{\partial R} + \frac{\partial^2 \overline{T}}{\partial R^2}\right] + \frac{\rho_B A_C L}{F_{T,0} T_0\left(\sum C_{Pi}\overline{F_i}\right)}\sum\left(R_i\left(-\Delta H_{ri}\right)\right) \tag{D-24}$$

B.C. $\overline{Z} = 0$; $\qquad \overline{T} = 1$ $\qquad (0 < R < 1)$

$\qquad R = 0$; $\qquad \dfrac{\partial \overline{T}}{\partial R} = 0$ $\qquad 0 < \overline{Z} < 1$

$\qquad R = 1$; $\qquad -\dfrac{2\pi L \lambda_{er}}{A_P}\dfrac{\partial \overline{T}}{\partial R} = U_{SS}\left(\overline{T}_{R=1} - \overline{T_j}\right)$ $\qquad 0 < \overline{Z} < 1$

3.2 Inert membrane reactor

$$A_{Cs} = \pi\left(r_3^2 - r_2^2\right) \qquad A_{Ct} = \pi r_1^2 \qquad A_{P1} = 2\pi r_1 L \qquad A_{P2} = 2\pi r_2 L$$

$$A_{P3} = 2\pi r_3 L$$

<u>Plug flow model</u>

Shell side:

$$\frac{d\overline{F_i^s}}{d\overline{Z}} = \frac{\rho_B A_{Cs} L}{F_{T,0}^s} r_i + \frac{L}{F_{T,0}^s}\left(\frac{F_i}{L}\right)' \tag{D-25}$$

$$\sum\left(\overline{F_i^s}C_{pi}\right)\frac{d\overline{T_s}}{d\overline{Z}} = \frac{U_{SS}A_{P3}}{F_{T,0}^s}(\overline{T_j}-\overline{T_s}) - \frac{U_M A_{P1}}{F_{T,0}^s}(\overline{T_s}-\gamma_1\overline{T_t})$$

$$+\sum\frac{L}{F_{T,0}^s T_{s,0}}\left(\frac{F_i}{L}\right)' H_i + \frac{A_{Cs}L}{F_{T,0}^s T_{s,0}}\rho_B\sum\left(R_i(-\Delta H_{ri})\right) \tag{D-26}$$

Tube side:

$$\frac{d\overline{F_i^t}}{d\overline{Z}} = -\frac{L}{F_{T,0}^t}\left(\frac{F_i}{L}\right)' \tag{D-27}$$

$$\sum\left(\overline{F_i^t}C_{pi}\right)\frac{d\overline{T_t}}{d\overline{Z}} = \frac{U_M A_{P1}}{F_{T,0}^t}(\gamma_2\overline{T_s}-\overline{T_t}) + \sum\frac{L}{F_{T,0}^t T_{t,0}}\left(\frac{F_i}{L}\right)' H_i \tag{D-28}$$

<u>Radial diffusion model</u>

Shell side:

$$\frac{\partial\overline{F_i^s}}{\partial\overline{Z}} = \alpha_{IMR,s}\left[\frac{1}{(R_s+R_2)}\frac{\partial}{\partial R_s}\left(\frac{\overline{F_i^s}}{\overline{F_T^s}\,\overline{T}}\right) + \frac{\partial^2}{\partial R_s^2}\left(\frac{\overline{F_i^s}}{\overline{F_T^s}\,\overline{T}}\right)\right] \tag{D-29}$$

$$+\frac{A_{Cs}L\rho_B}{F_{T,0}}r_i$$

B.C. $\overline{Z}=0$; $\quad\overline{F_i^s}=\overline{F_{i,0}^s}\quad (0<R_s<1)$

$\quad R_s=0$; $\quad -D_{er}^s\dfrac{P_s}{R_{gas}T_{s,0}}\dfrac{d}{dR_s}\left(\dfrac{\overline{F_i^s}}{\overline{F_T^s}\,\overline{T_s}}\right) = \dfrac{L}{A_{P2}}\left(\dfrac{F_i}{L}\right)'\ 0<\overline{Z}<1$

$\quad R_s=1$; $\quad \dfrac{\partial}{\partial R_s}\left(\dfrac{\overline{F_i^s}}{\overline{F_T^s}\,\overline{T_s}}\right) = 0 \qquad 0<\overline{Z}<1$

$$\frac{\partial\overline{T_s}}{\partial\overline{Z}} = \beta_{IMR,s}\left[\left(\frac{1}{R_s+R_2}\right)\frac{\partial\overline{T_s}}{\partial R_s} + \frac{\partial^2\overline{T_s}}{\partial R_s^2}\right] + \frac{\rho_B A_{Cs}L}{F_{T,0}^s T_{s,0}\left(\sum C_{Pi}\overline{F_i^s}\right)}\sum\left(R_i(-\Delta H_{ri})\right) \tag{D-30}$$

$\qquad\overline{Z}=0$; $\qquad \overline{T_s}=1 \qquad (0<R_s<1)$

$\qquad R_s=0$;

$$-\frac{\lambda_{er}^{s}\pi}{A_{C_s}}\frac{\partial \overline{T_s}}{\partial R_s} = U_M\left(\gamma_1 \overline{T_t}_{R_t=1} - \overline{T_s}_{R_s=0}\right) + \sum \frac{L}{A_{P2}T_{s,0}}\left(\frac{F_i}{L}\right)' H_i$$

$$R_s = 1;\qquad -\frac{\lambda_{er}^{s}\pi}{A_{C_s}}\frac{\partial \overline{T_s}}{\partial R_s} = U_{SS}\left(\overline{T_s}_{R_s=1} - \overline{T_j}\right) \qquad 0 < \overline{Z} < 1$$

VITA

Mr. Tavorn Rienchalanusarn was born in Bangkok on September 25, 1976. He received the Bachelor degree of chemical engineering from the Department of Chemical Engineering, Faculty of Engineering, King Mongkut's Institute of Technology Ladkrabang (KMITL) in 1998.